ACS APPLIED MATERIALS & INTERFACES

www.acsami.org Research Article

Preclinical Development of Magnetic Nanoparticles for Hyperthermia Treatment of Pancreatic Cancer

Zamira V. Díaz-Riascos, Monserrat Llaguno-Munive, Nuria Lafuente-Gómez, Yurena Luengo, Sarah Holmes, Jeanne Volatron, Oihane Ibarrola, Sandra Mancilla, Francesca Sarno, José Javier Aguirre, Sarah Razafindrakoto, Paul Southern, Francisco J. Terán, Anna Keogh, Gorka Salas, Adriele Prina-Mello, Juan Carlos Lacal, Angel del Pozo, Quentin A. Pankhurst, Manuel Hidalgo, Florence Gazeau, Álvaro Somoza, Simó Schwartz, Jr.,* and Ibane Abasolo*

Cite This: https://doi.org/10.1021/acsami.4c16129 Read Online

ACCESS | Metrics & More | Article Recommendations | Supporting Information

ABSTRACT: Pancreatic ductal adenocarcinoma (PDAC) is a very challenging disease with a very poor prognosis. It is characterized by a dense desmoplastic stroma that hampers drug penetration and limits the effectiveness of conventional chemotherapy (CT). As an alternative, the combination of CT with hyperthermia (HT) has been proposed as an innovative treatment modality for PDAC. In previous works, we reported on the development of iron oxide magnetic nanoparticles (MNPs) that, when exposed to time-varying magnetic fields, exhibit strong HT responses that inhibited the growth of pancreatic cancers. We report here on advances toward the clinical use of these MNPs as an intratumorally administered sterile magnetic fluid (the "NoCanTher ThermoTherapy" or "NTT" Agent) alongside intravenous standard-of-care drugs (gemcitabine and nab-paclitaxel) for the treatment of PDAC. *In vitro* cell viability assays show that the combination of low doses of CT and HT is highly synergistic, particularly in the BxPC-3 cell line. *In vivo*, biodistribution assays showed that the NTT Agent MNPs remained mainly within the tumor, concentrated around areas with a high stromal component. Moreover, the combined CT/HT treatment shows clear advantages over CT alone in terms of drug penetration and reduction of the tumor volume, suggesting a potential direct effect of HT in the disruption of the interstitial stroma to facilitate the access of the drugs to malignant cells. These studies have led to the approval and commencement of a clinical investigational study at the Vall d'Hebron University Hospital (Barcelona, Spain) of the NTT Agent alongside CT in patients with locally advanced PDAC.

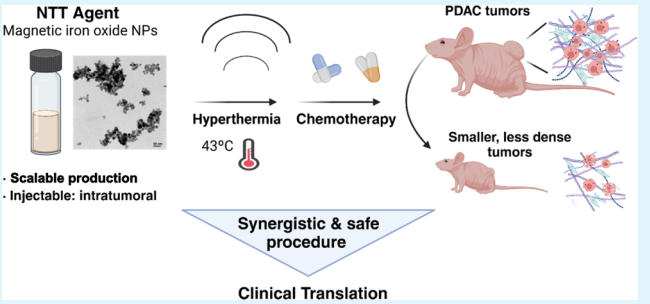

KEYWORDS: *alternating magnetic field, chemotherapy, combination therapy, iron oxide nanoparticles, hyperthermia, nanoparticle biodistribution, pancreatic cancer*

1. INTRODUCTION

Pancreatic cancer remains one of the deadliest cancers and the seventh leading cause of cancer death worldwide.[1] The prognosis of pancreatic ductal adenocarcinoma (PDAC) is very poor. With an average annual death rate of 11.2/100,000, despite the advances in treatment, the survival rates of pancreatic cancer have not changed in 40 years. Currently, surgical resection is the only chance for a cure. Unfortunately, 80−85% of patients present with advanced unresectable disease at the time of diagnosis.[2] Regarding chemotherapy (CT), first-line palliative regimens with FOLFIRINOX or gemcitabine/nab-paclitaxel (GEM/nab-PTX) have become the standard-of-care over the past decade.[3,4] In the second-line setting, 5-fluorouracil and lecovorin (5FU/LV) in combination with nanoliposomal irinotecan after gemcitabine have been shown to be effective.[5] However, due to the abundant interstitial stroma surrounding the cancer cells[6] and the irregular blood supply that characterizes most pancreatic tumors,[7] pancreatic cancer responds poorly to most of the CT agents.[8] In this context, and especially after observing the limited benefit of immunotherapy in PDAC,[9] many experimental protocols include the use of combined CT agents in association with agents targeting specific molecular pathways (i.e., fibroblast growth factor (FGF), vascular endothelial growth factor (VEGF), and farnesyl-transferase inhibition) with the aim of facilitating the access of the cytostatic drug to malignant cells.[10]

Received: September 20, 2024
Revised: November 25, 2024
Accepted: November 26, 2024

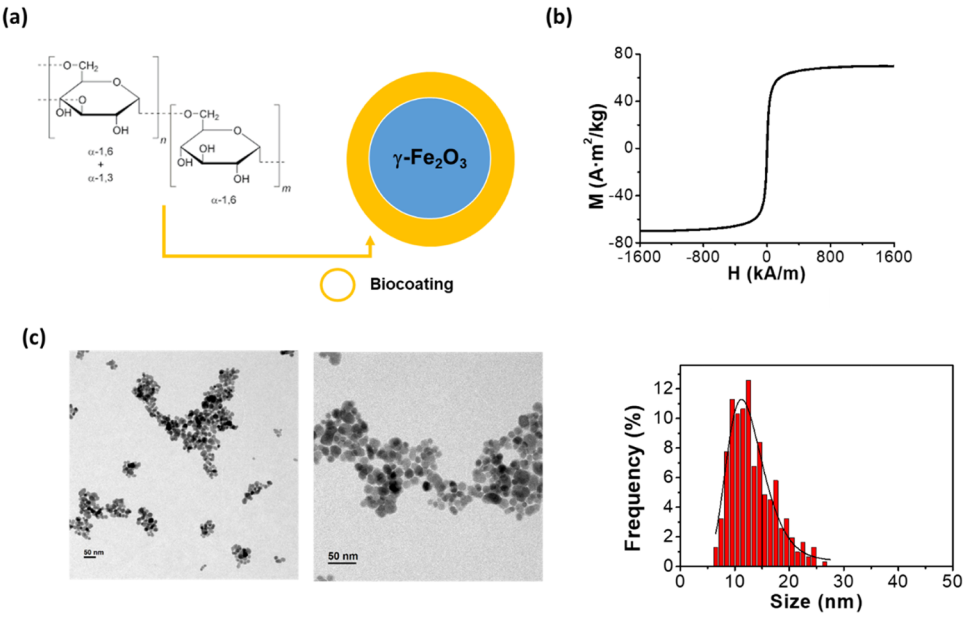

(d)

Size		PdI	Z-pot (mV)	SLP (W/g_{Fe})	
TEM (nm)	Z-average (nm)			300 kHz, 4 kA/m	100 kHz, 24 kA/m
14 ± 4	103 ± 16	0.27± 0.09	-10 ± 5	6 ± 1	131 ± 32

Figure 1. NTT Agent physicochemical characterization: (a) Scheme of the NTT Agent with the dextran coating; (b) Field (H)-dependent magnetization (M) of the NTT agent measured by vibrating sample magnetometry. (c) Representative images of transmission electron microscopy (TEM) showing the morphology and size of NTT Agent nanoparticles and the size distribution obtained from TEM images. (d) Summary of the size, surface charge, and specific loss power (SLP) of the NTT Agent. Values correspond to the mean and standard deviation (SD) of 3−5 different batches.

In this scenario, magnetic hyperthermia (HT) may offer the advantage of combining its intrinsic antitumoral efficacy with the ability to disrupt the stromal barrier.[11−13] On the one hand, previous results showed that the use of alternating magnetic fields (AMF) on magnetic nanoparticles (MNP) sensitizes tumor cells to CT.[14,15] On the other hand, nanoparticle-based HT has been shown to modulate the tumor extracellular matrix by altering the organization of collagen fibers and allowing for better drug penetration.[16,17] In HT treatments, the temperature is usually raised above 45 °C, but mild HT where the temperature is kept below 43 °C has also shown benefits, directly affecting the tumor vasculature,[18] matrix, and immunomodulation.[19,20] It is also important to note that HT can be fine-tuned when using the right combination of nanoparticles and AMF strength and frequency.[21] It is widely accepted that the temperature of 43 °C for 60 min inactivates tumor cells and the use of lower temperatures for shorter times might also work.[22] However, there are still many variables that need to be controlled to increase the efficacy of HT and CT combinations, including the dose of the drug, the intensity of the heating, and the time lapse between the heat application and CT.[23,24] These difficulties might explain the limited permeation of magnetic HT into clinical practice, with just one MNP formulation currently approved for clinical HT: NanoTherm (MagForce AG, Berlin, Germany).[24]

In the present work, our main objective is to advance in the preclinical development of MNPs developed under the NoCanTher consortium (EU-funded Project GA685795) in the form of an intratumorally administered sterile magnetic fluid (the "NoCanTher ThermoTherapy" or "NTT" Agent). First, dextran-coated nanoparticles were synthesized and characterized by following procedures that allowed direct escalation of the production procedures. *In vitro*, the NTT Agent showed a good heating potential and direct antiproliferative effects in pancreatic cancer cell lines. Safety assays, including *in vivo* tolerability and biodistribution assays, were performed. Subsequently, efficacy assays using suboptimal doses of gemcitabine and nab-PTX demonstrated that the addition of HT reduced tumor growth to a greater extent than the chemotherapy alone. Based on these results, clinical investigational studies were initiated (797/20/EC)[25] at the Vall d'Hebron University Hospital (Barcelona, Spain) to test the safety and feasibility of using the NTT Agent in combination with CT for the treatment of locally advanced PDAC.

2. RESULTS AND DISCUSSION

2.1. Magnetic Nanoparticle Synthesis and Characterization. With the clear goal of developing a clinically useful magnetic HT treatment, we have synthesized and characterized a sterile and biocompatible magnetic fluid, the "NTT Agent", which is suitable for intratumoral administration and which contains all of the requirements in terms of nanoparticle uniformity, heating capability (SLP values), and clinical scalability (Figure 1). As the solid-matter part of the NTT Agent, both single-core and multicore MNPs were prepared by the coprecipitation technique[26] and coated with dextran-40 (Figure 1) according to previously described procedures.[21] The data described in this paper relate to an NTT Agent formulation containing single-core MNPs comprising iron

https://doi.org/10.1021/acsami.4c16129
ACS Appl. Mater. Interfaces XXXX, XXX, XXX−XXX

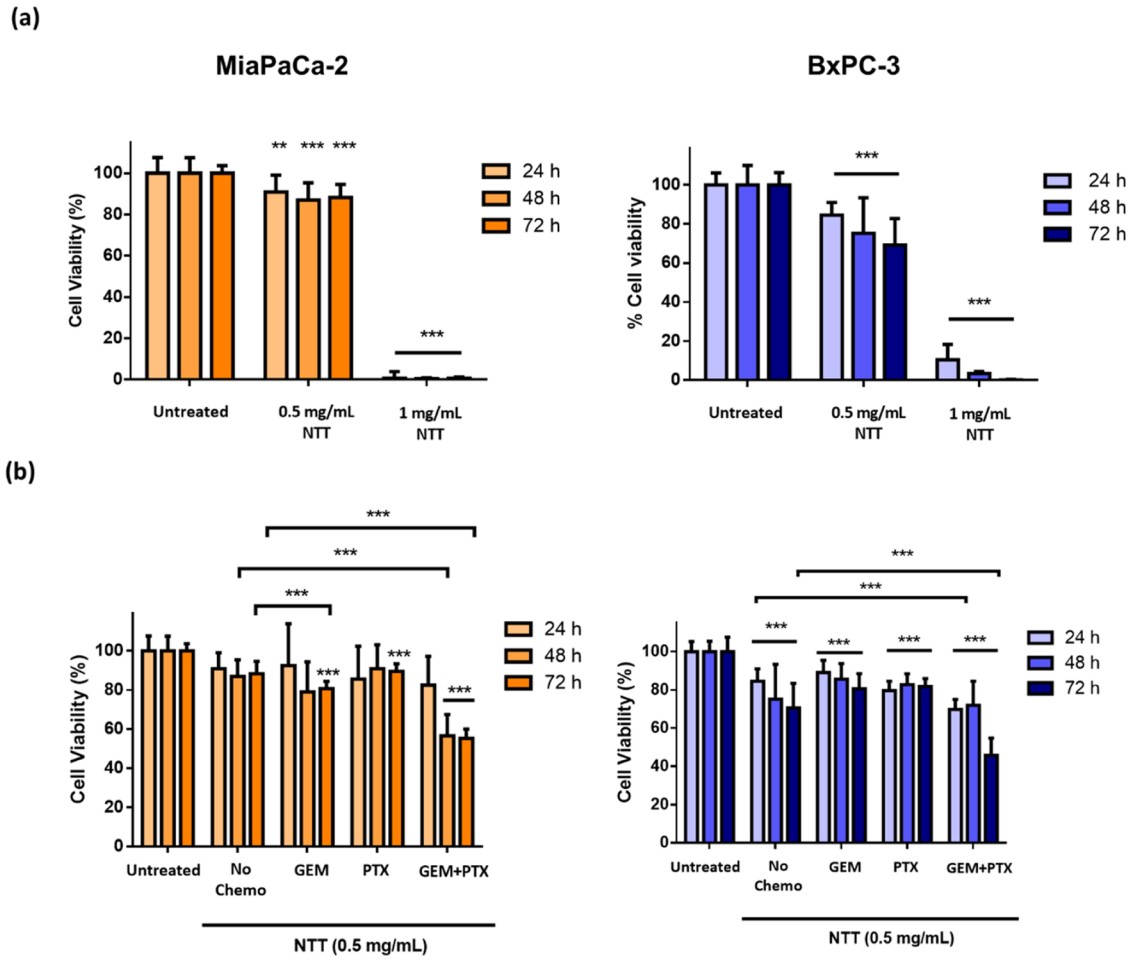

Figure 2. *In vitro* effect after magnetic hyperthermia in pancreatic human cancer cell lines. (a) Effect of the MNPs with AMF in MiaPaCa-2 and BxPC-3 cells, showing that the NTT effect increases with the dose. (b) Combination of the NTT Agent at 0.5 mg/mL with GEM (0.01 μM) and PTX (0.01 μM) in MiaPaCa-2 and BxPC-3 cells. Values correspond to the average of at least 3 independent experiments. Comparisons are made against the untreated cells or among groups indicated by the square bracket and significance levels were schematically assigned: *$0.01 \leq P < 0.05$, **$0.001 \leq P < 0.01$, and ***$0.0001 \leq P$..

oxide (maghemite) cores coated with dextran-40 (Figure 1a); data on another NTT Agent formulation containing multicore MNPs is available elsewhere.[27−29]

Critical manufacturing parameters (such as pH, excipients, particle aggregate size, Fe content, specific loss power, thermogravimetric analysis, bacterial endotoxins, and temperature ranges) were fine-tuned to enable multigram-scale production that complied with required quality attributes and batch-to-batch consistency. This batch-to-batch consistency was of utmost importance, allowing quality controls to be established, in accordance with the ISO 13485 Quality Management System in the Design and Manufacture of Medical Devices and Medical Devices Directive 93/42/EEC. Release criteria for the NTT Agent were set as pH = 5.5−7.5; particle aggregate size = 90−180 nm; aggregate size distribution SPAN = $(D90-D10)/D50 \leq 1.2$ (where DN is the size of D of the Nth percentile of the particle aggregate size probability distribution); Fe content ≥ 50 mg_{Fe}/mL; bacterial endotoxins ≤ 1,6 EU/mg; specific loss power ≥ 10 W/g_{Fe} (measured in 24 kA/m, 100 kHz AMF); and dextran content ≥ 10% (W7W) as measured by thermogravimetric analysis. Among all of the production batches, the iron oxide cores exhibited a nearly spherical uniform shape with mean diameters of 14 ± 4 nm, as measured by TEM (Figure 1). This result is typical of single-core MNPs prepared by coprecipitation[30] and in excellent agreement with previous publications, as expected due to the high reproducibility of the coprecipitation synthesis method.[21] The aggregation of MNPs was also studied in 6 different production batches. This showed that the aggregates were kept within a relatively tight range of average sizes, 103 ± 16 nm, with a rather small polydispersity index (PdI) of 0.27 ± 0.09. The ζ-potential as measured by dynamic light scattering (DLS) fell in the range of −10 ± 5 mV (Figure 1d).

The long-term stability of the nanoparticles was assessed according to both nonregulatory and regulatory guidelines, including the ISO 13485 Quality Management System, the Medical Devices Directive 93/42/EEC, and ASTM F1980-16 for Accelerated Aging of Sterile Barrier Systems in Medical Devices. For the nonregulatory evaluation, three MNP batches with iron concentrations of 20, 40, and 60 mg_{Fe}/mL were stored at 4 °C. Their hydrodynamic sizes (Z-average) and PdIs were monitored by DLS over an 18-month period. Measurements were taken at 25 °C by diluting an aliquot from each refrigerated sample. Results, presented in Table S1 and Figure S1, demonstrate consistent hydrodynamic sizes within a range of 100−160 nm, predominantly around 100 nm, and PdI

https://doi.org/10.1021/acsami.4c16129
ACS Appl. Mater. Interfaces XXXX, XXX, XXX−XXX

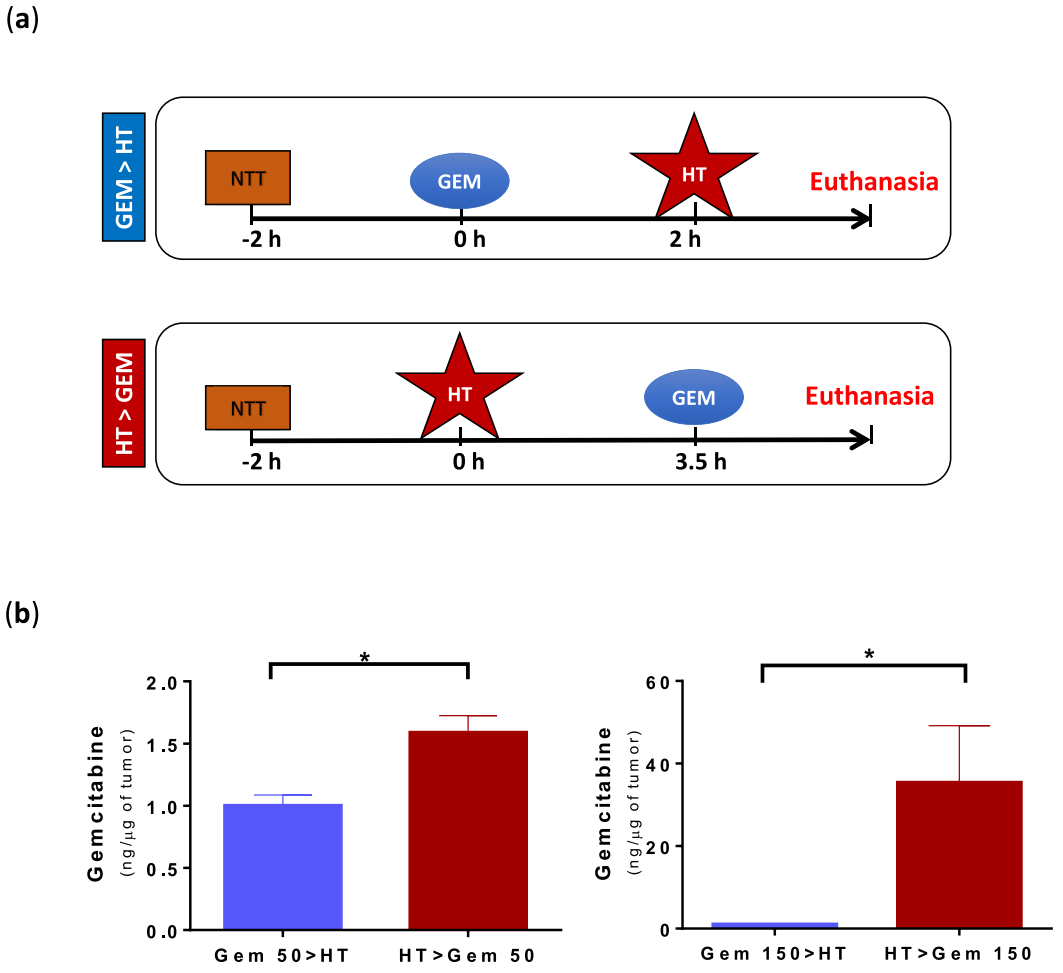

Figure 3. Gemcitabine (GEM) accumulation in PDX tumors depends on the dose and sequence of treatments. (a) Scheme of the treatment sequences. MNPs were administered intratumorally (1 mg Fe/100 mm^3 of tumor), and animals were euthanized 24 h after GEM administration. (b) GEM levels determined by liquid chromatography and tandem mass spectrometry (LC-MS/MS) in tumors of animals that received 50 or 150 mg/kg of the drug, before or after applying the AMF to induce HT. The threshold for significance was $P < 0.05$ (*) and $P < 0.01$ (**).

values ranging from 0.09 to 0.24 for all samples throughout the aging study period.

Long-term stability under regulatory conditions was evaluated by storing samples at 5 °C for 24 months and under accelerated aging conditions during 6 months at 25 ± 2 °C to simulate storage up to 2 years at 5 °C (see Tables S2 and S3). The results from these regulatory studies indicate that the samples meet all specified criteria under both standard and accelerated aging conditions. The observed changes in measured parameters remain within acceptable limits, confirming that the NTT Agent retains stability over time.

In addition, the heating capability of the MNPs was evaluated in terms of the specific loss power (SLP) metric. This parameter was quantified by measuring three times the dynamic hysteresis loops at different field and frequency conditions (4 kA/m, 300 kHz; 24 kA/m, 100 kHz).[21] As expected, SLP values increased with the higher field intensity conditions, from 6 ± 1 W/g_{Fe} at 4 kA/m, 300 kHz to 131 ± 32 W/g_{Fe} at 24 kA/m, 100 kHz using magnetic dispersions with [Fe] = 1 mg_{Fe}/mL.

2.2. *In Vitro* Effect of AMF Alone or in Combination with GEM and PTX in Pancreatic Cancer Cells. Considering that in the clinical setting, the NTT Agent would most likely be administered in combination with first-line treatments in PDAC patients,[24] the safety and efficacy of the magnetic HT in combination with the standard-of-care drug treatment had to be tested in PDAC preclinical models. As mentioned above, the combination of HT with radiotherapy (RT) or chemotherapy (CT) has become an important strategy to increase the therapeutic response in various cancers.[24,31,32] Many studies have shown that by adding HT to CT, the delivery and efficacy of the drug to the tumor is improved as the heat increases cellular permeability and sensitizes tumors to the chemotherapeutic drugs.[14,33,34] To test this hypothesis, we first evaluated the efficacy of the NNT Agent as a solo treatment in PDAC cell lines. In detail, pancreatic MiaPaCa-2 and BxPC-3 cancer cells were incubated with the NTT Agent (0.5 and 1 mg Fe/mL) for different time points, washed with phosphate-buffered saline (PBS), and subjected to AMF for 20 min (Figure 2a) to evaluate the efficacy of the HT driven by the MNPs. The results showed that when cells were treated with 1 mg of Fe/mL plus the AMF (23.8 kA/m and a frequency of 202 kHz), the cell viability of both cell lines fell to below 10%, 72 h after the treatment. Lower NTT doses, such as 0.5 mg of Fe/mL followed by the AMF, also reduced cell viability but to a lower extent: 90% in MiaPaCa-2 cells and 70−80% in BxPC-3 cells, indicating that HT is capable of inducing cell death in a dose-dependent

https://doi.org/10.1021/acsami.4c16129
ACS Appl. Mater. Interfaces XXXX, XXX, XXX−XXX

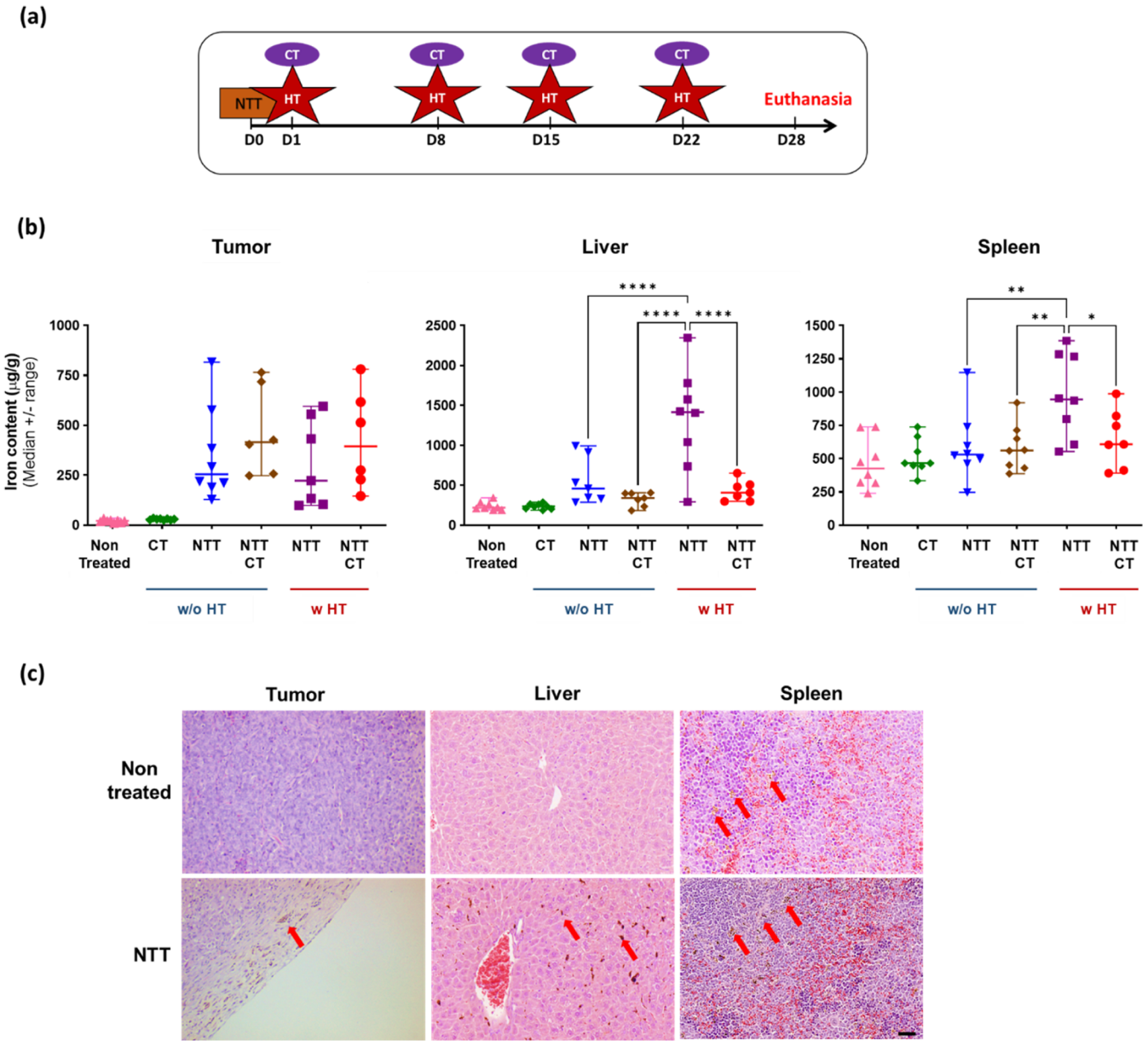

Figure 4. Safety and biodistribution of NTT Agent after HT/CT combination therapy in animals with subcutaneous MiaPaCa-2 tumors. (a) Assay schedule, including intratumoral administration of the MNPs (the NTT Agent) and magnetic hyperthermia (HT) followed by treatment with chemotherapy (CT, 3.5 h post-HT). (b) Iron determinations by inductively coupled plasma mass spectrometry (ICP-MS) in different organs. Graphs show the mass of iron per organ in each individual (individual dots), the median (line), and the range (error bars). The number of animals was ranging between $n = 6$ and 8 per group. Statistical comparisons were conducted among NTT-administered groups and significant differences are shown with $P < 0.05$ (*), $P < 0.01$ (**), $P < 0.001$ (***), and $P < 0.0001$. (c) Histological evaluation on H−E-stained paraffin sections showed the iron deposits (red arrows) in different tissues. Magnification bar in the last image corresponds to 50 μm and applies to all images.

manner. Meanwhile, the treatment of the cells by the addition of the NTT Agent without the application of the AMF did not cause any significant cell death (Figure S2).

Next, we studied whether HT induced any chemosensitization in pancreatic cancer cells. To that end, cell viability was determined in MiaPaCa-2 and BxPC-3 cells immediately after AMF (0 h), and at 24 and 48 h after completion of HT, these three time points correspond to 24, 48, and 72 h after treatment with GEM and PTX, respectively. In these assays, chemotherapeutics were employed at a suboptimal dose (0.01 μM) that did not compromise the cell viability significantly by themselves (see Figure S2). The results in Figure 2b show that in both cell lines, the combination of the chemotherapy with the HT significantly reduced the cell viability, especially when both drugs, GEM and PTX, were used simultaneously. For instance, BxPC-3 cells receiving combination therapy of NTT Agent + GEM + PTX and the AMF had an overall cell viability of 45.9 ± 8.8% at 72 h, while cell viability was at 70.6 ± 12.8% for the cells receiving only the NTT Agent with the AMF-induced HT.

Consistent with prior studies,[14,33,34] our *in vitro* results demonstrate that the addition of standard-of-care drugs, GEM and PTX, to pancreatic cancer cells also treated with MNP-enabled HT significantly reduces cell viability compared to treatments with HT or CT alone (Figure 2). While the exact mechanisms behind this synergistic effect in the combined

https://doi.org/10.1021/acsami.4c16129
ACS Appl. Mater. Interfaces XXXX, XXX, XXX−XXX

HT/CT treatment are not fully understood, several potential mechanisms have been described in the literature. At the cellular level, HT has been reported to induce direct physical damage to DNA,[35,36] and to cell and lysosomal membranes,[37,38] to disrupts the cell cytoskeleton[39] to alter calcium ion influx,[40] and induces signal transduction,[41] and to lead to stress-induced gene expression.[42,43] In contrast, the chemotherapeutic agents GEM and PTX are known to interfere with DNA synthesis[44] and microtubule formation.[45] It is perhaps notable here that the CT-induced cellular death mechanisms do not completely overlap with those induced by HT, which might explain the synergistic adjuvant effects observed between the two treatments.

2.3. Combination of CT with HT in PDX Models. In a real-world context, the effect of magnetic HT is not limited to the cancer cells, and the tumor response to HT also involves changes in the vasculature, immune cell response, and extracellular matrix modifications that cannot be studied using conventional two-dimensional (2D) cell cultures. Although three-dimensional (3D) models have also been used to optimize the AMF protocols,[46,47] these models cannot fully explain the intratumoral distribution of nanoparticles and the overall temperature increases, and *in vivo* experiments are needed. Previous work by Luengo et al.[21] showed that it is possible to control the temperature increase in mice with intratumoral administration of MNPs. Building on this, we further explored the optimal sequencing of HT and CT in animals undergoing a single cycle of combined HT/CT treatment. This step was essential as clinical trials with nonmagnetic HT and CT have not yet clarified the ideal timing for drug administration relative to HT treatment.[48]

Employing patient-derived xenograft (PDX) models, which more closely resemble the phenotypic characteristic of PDAC patient tumors,[49−51] we studied whether the CT/HT sequence affects the retention of the chemotherapeutic drug within the tumor. In detail, mice bearing pancreatic cancer PDX were first administered with MNP at 1 mg of Fe per 100 mm^3 tumor volume and then divided into two treatment groups. Half of the animals (n = 6) received two different doses of GEM, 50 and 150 mg/kg intraperitoneally (i.p.) 2 h before HT treatment and the other half of the animals (n = 6) received the GEM dose after HT treatment. In both cases, the animals were euthanized 24 h after GEM administration (Figure 3a). A "MACH" system (*viz* a "Magnetic AC Hyperthermia" magnetic field generation system, manufactured by Resonant Circuits Limited, London) equivalent to the one used in clinical studies was adapted to work with experimental animals (Figure S3). GEM determinations by liquid chromatography-mass spectrometry (LC-MS) in tumors showed significantly higher chemotherapeutic drug content when CT was administered after (rather than before) HT (Figure 3b). Although the difference between the two types of sequences was greater at the 150 mg/kg GEM dose, the differences were also statistically significant at the lower dose of 50 mg/kg. These results demonstrated that the administration of the CT (GEM) after the HT resulted in a higher accumulation of the drug within the tumors and were used to define the HT/CT sequence in the following experiments, where the CT was always administered between 2 and 3.5 h post-HT.

The higher drug accumulation when HT is delivered before the CT might be caused (at least in part) by the mild increase in the tumor temperature, which improves the blood flow in the tumor and favors the extravasation of the drug. Preclinical studies using HIPEC (hyperthermic intraperitoneal CT) protocols, in which GEM is heated to 41−43 °C and administered intraperitoneally, have also shown that adsorption and intracellular uptake of GEM is favored by the increased temperatures.[52] HIPEC, as well as MNP-driven HT, has also demonstrated that the use of the heat reduces the number of cancer stem cells[53] and circulating tumor cells in PDAC,[27] meaning that the use of HT in combination with the standard-of-care drugs may also play a direct role in reducing the aggressiveness and progression of PDAC.

2.4. NTT Agent Safety and Biodistribution in Mice Bearing Pancreatic Tumors. Once we had established the sequence of HT and CT, we continued to evaluate the *in vivo* biodistribution and safety of the NTT Agent after intratumoral administration in MiaPaCa-2 subcutaneous (s.c.) tumors. The NTT Agent was inoculated intratumorally at day 0, and HT/CT was applied weekly for 4 weeks before euthanasia (Figure 4a) using the MACH system (Figure S3). The route of administration as well as the combination with the CT was carefully chosen to mimic the anticipated clinical situation, where the NTT Agent would be administered intratumorally (via an endoscope located in the stomach and guided by echography/ultrasound) and patients would receive the CT on the day after NTT Agent administration. As for the dose of CT, a preliminary assay was conducted to select the minimal doses of GEM and nab-PTX (the standard-of-care CT drugs in PDAC patients), that would render a significant reduction in tumor volume after 3 weeks of treatment in mice (see Figure S4a). The selected CT of GEM and nab-PTX thus determined corresponded to the murine concentrations of 10 and 5 mg/kg, respectively.

Animal welfare was monitored throughout the treatment by closely monitoring rectal and surface temperatures of the animals during HT as well as by registering the general appearance, response to stimuli, and body weight. Overall, animals treated with NTT alone or in combination with chemotherapeutic drugs showed no adverse effect, and both the HT and the CT regimens were well-tolerated (weight loss less than 10% in all treatment groups). It was also confirmed that the MNP administration alone, without the application of AMF did not induce any change in the growth of the tumors (Figure S4b), in agreement with previous results.[14,54]

At the end of the experiment, total iron levels in the different tissues were measured by inductively coupled plasma mass spectrometry (ICP-MS) (Figure 4b). The superparamagnetic iron fraction coming from AMF-responsive heating-capable MNPs was also quantified by electron paramagnetic resonance (EPR) for comparison (Figure S5) as previously described.[55] Tumors from control animals not treated with the NTT Agent had very low levels of endogenous iron (21 ± 3 $\mu g_{Fe}/g_{tumor}$, mean ± SEM), while tumors from NTT Agent-treated animals had 10 times higher levels of iron (306 ± 83 $\mu g_{Fe}/g_{tumor}$), thus comprising both the endogenous iron plus the iron coming from the NTT Agent. EPR quantification showed that the iron in the tumor, even after 4 rounds of HT, was mostly superparamagnetic, meaning that tumors still contained heating-capable NTT Agent nanoparticles. In contrast to the tumor, basal iron levels in the liver and spleen of untreated mice (240 ± 19 and 465 ± 67 $\mu g_{Fe}/g_{tissue}$, respectively) were only moderately different to those in NTT Agent-treated animals (552 ± 109 and 594 ± 93 $\mu g_{Fe}/g_{tissue}$, respectively), and the liver and spleen contained only small amounts of superparamagnetic MNPs (Figure S5). This indicates that the

https://doi.org/10.1021/acsami.4c16129
ACS Appl. Mater. Interfaces XXXX, XXX, XXX−XXX

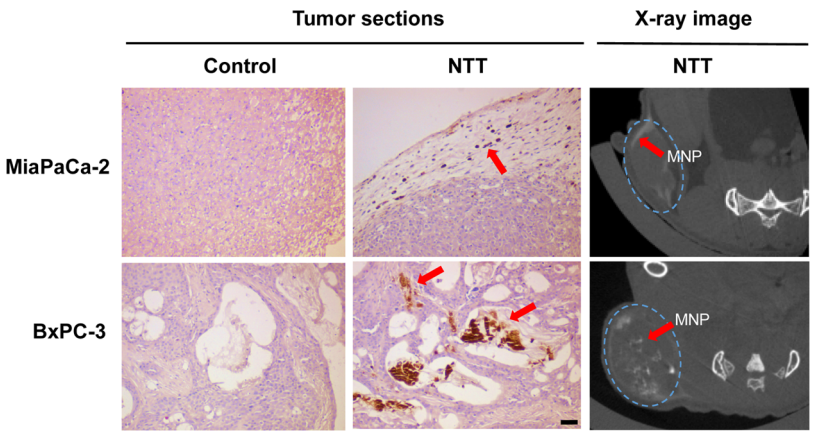

Figure 5. Intratumoral biodistribution of the NTT Agent MNPs in two subcutaneous models of pancreatic cancer, MiaPaCa-2 and BxPC-3. The MNPs were visualized in sections of the formalin-fixed paraffin-embedded (FFPE) material, as shown by the brown precipitates in the capsule surrounding the MiaPaCa-2 tumor or in the interstitial spaces of the BxPC-3 tumors. Such brown precipitates did not appear in the control animals that did not receive the NTT Agent. Magnification bar in the last image corresponds to 50 μm and applies to all images. X-ray computed tomography images show coronal sections of the animal, with the tumor shown on the left side. The dotted blue line indicates the tumor margin, and the red arrows point to MNP deposits either inside the tumor or in the surrounding subcutaneous space.

release and diffusion of the intratumorally injected NTT Agent from the tumor to the spleen and liver were relatively low. Interestingly, HT in mice with intratumor administration of the NTT Agent moderately altered the distribution of MNPs in the body, increasing by 3- and 1.6-fold the levels of iron in liver and spleen, respectively, when compared with the animals receiving the NTT Agent alone, without any HT. Notably, CT incorporation did not increase nanoparticles leakage into the liver or other organs, as no differences were observed when comparing iron levels in mice receiving MNP and CT without HT and those receiving the complete treatment combining HT and CT.

Histological analysis confirmed the safety of the HT/CT treatment (Figure 4c). No macroscopic or microscopic alterations related to the treatment were observed outside the tumors. Brownish deposits corresponding to iron oxide nanoparticles could be observed in tumors (mainly in the tumor capsule and not that much in the interior of the tumor) as well as in the liver and spleen of NTT Agent-treated animals, as later confirmed by Prussian blue staining. The livers of NTT Agent-treated animals showed the presence of abundant Kupffer cells loaded with brownish iron, indicating a clearance of MNPs from the tumor. In some areas of the liver, some globoid degeneration in the lobular hepatocytes could be observed in mice receiving MNP.

Overall, these findings indicate that, unlike intravenous injection—where the majority of injected MNPs accumulate in the liver, kidneys, and spleen[14,56]—intratumoral administration of nanoparticles reduces clearance by the reticuloendothelial system (RES), resulting in higher intratumoral MNP concentrations and an enhanced therapeutic impact on tumor growth.[28,57,58] In our study, 4 weeks postadministration, the NTT Agent exhibited the following characteristics: (i) MNPs remained localized within the tumor, retaining their superparamagnetic properties essential for heating under AMF exposure; (ii) neither CT, HT, nor their combination significantly affected the presence of MNPs within the tumor; and (iii) the presence of superparamagnetic MNPs outside the tumor was minimal. Importantly, if any heating occurred in tissues outside the tumor, it was undetectable by histological analysis and had no adverse impact on animal welfare.

2.5. Intratumoral Distribution of NTT Agent Nanoparticles. Although MiaPaCa-2 s.c. tumors retained high levels of the NTT Agent, the efficacy in this model was limited (Figure S4b) and the temperatures recorded by optical probes on the tumor surface (spot temperatures) were barely above 40 °C (Figure S6a). Closer analysis of the H−E sections of MiaPaCa-2 tumors revealed that much of the NTT was retained in the tumor capsule and was not homogeneously distributed within the tumors (Figure 5). These results were confirmed by radiology (X-ray computed tomography) images of the mice taken 2 h after NTT Agent administration, which showed accumulation of MNPs in the subcutaneous space surrounding the tumor but not in the tumor itself. The same analysis performed in BxPC-3 sc tumors showed that the MNPs were better distributed within the tumor. Such increased presence of the NTT Agent in BxPC-3 s.c. tumors resulted in a better heating of these tumors compared to MiaPaCa-2 ones, when AMF was applied (Figure S6b). Thus, tumors with a less desmoplastic and more glandular structure allow a greater intratumoral concentration of the MNPs that then translated into a more significant heating potential. Differences in the MNP distribution depending on the tumor type have been previously described in the literature.[59] Indeed, such differences in the intratumoral accumulation of the MNP might be found also in the patients[60] and suggest that CT or MRI imaging of the MNP distribution could be used to predict the patient's response to the HT treatment.[61] Although the use of the NTT Agent as a theranostic nanomaterial was not the objective of this work, the visualization of the MNPs by CT confirms that this strategy could be eventually used in the clinical setting.

2.6. Efficacy of Magnetic HT in Combination with CT in BxPC-3 s.c. Models. Since BxPC-3 cells were more sensitive to the HT/CT combination and accumulated more NTT Agent inside the tumor than MiaPaCa-2, the therapeutic efficacy assay was performed in mice bearing s.c. BxPC-3 tumors (Figure 6). The NTT Agent was administered 2 h prior to HT treatment, and CT (10 and 50 mg/kg of nab-PTX and GEM, respectively) was administered 4 h later. The HT/CT

https://doi.org/10.1021/acsami.4c16129
ACS Appl. Mater. Interfaces XXXX, XXX, XXX−XXX

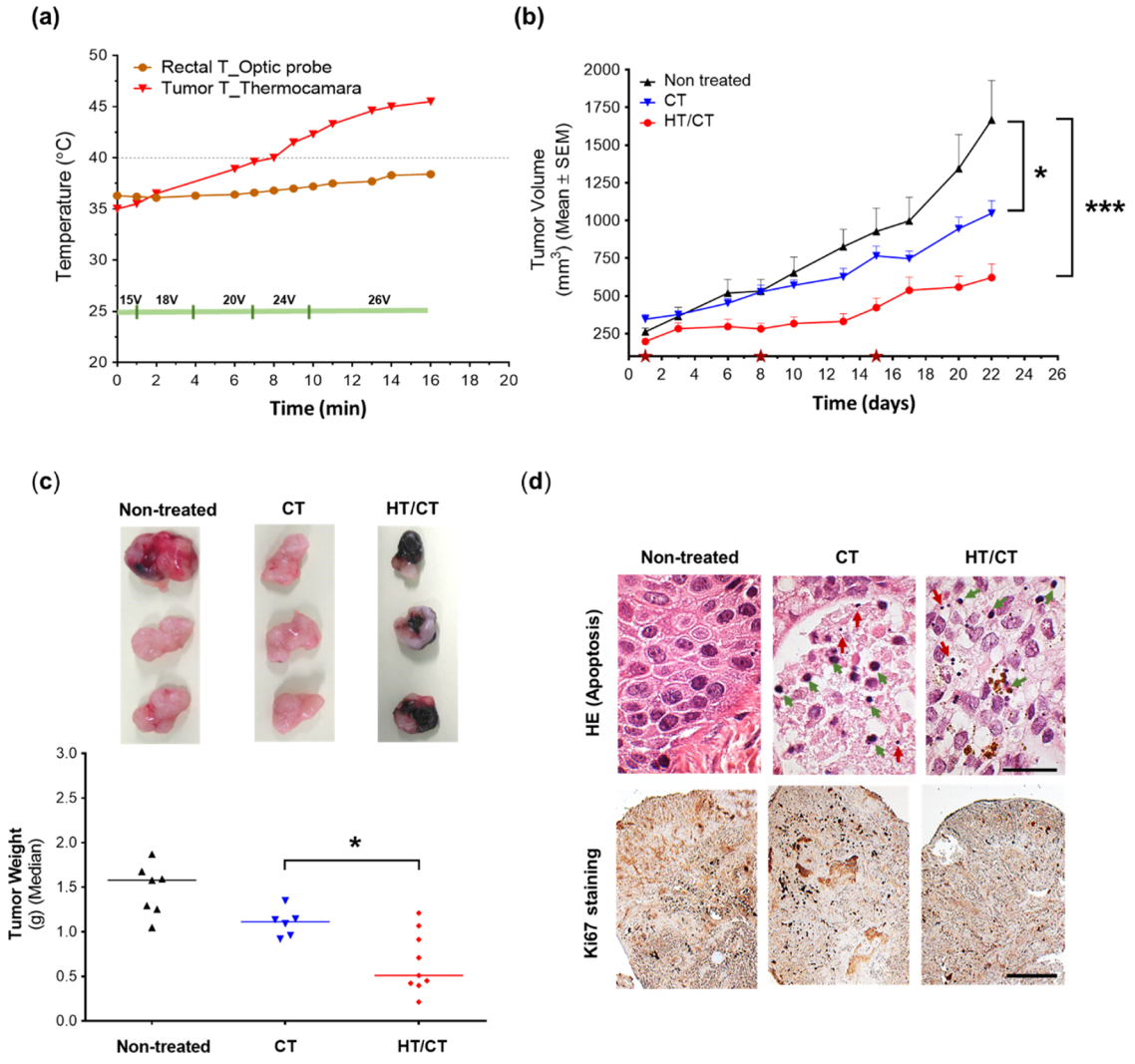

Figure 6. Efficacy of the HT/CT treatment in BxPC-3 sc tumors. (a) Temperature recordings in a representative case. Green line reflects the duration of each of the MACH magnetic field generator voltages applied during the HT protocol—these correspond to field strengths of 4.02, 4.98, 5.59, 6.74, and 7.27 kA/m at generator voltages of 15, 18, 20, 24, and 26 V, respectively. (b) Tumor volumes along the treatment. Red stars on the *x*-axis indicate the treatment days on which HT was delivered 2.5−3 h before CT (50 mg/kg GEM i.p. and 10 mg/kg nab-paclitaxel i.v.). (c) Tumor weight at the end of the experiment. (d) Apoptosis and proliferation in BxPC-3 tumors. In H−E images (top panel), green and red arrows indicate apoptotic bodies and white asterisks indicate cancer cells with iron deposits in their cytoplasm. Magnification bar in the last image corresponds to 50 μm in H−E images and 200 μm in Ki67 staining.

combination was repeated once a week for 3 weeks. In each HT treatment session, the heating of the tumor was controlled by adjusting the amplitude of the AMF from a starting point of 4.02 kA/m to a maximum of 7.27 kA/m (Figure 6a). In all cases, the AMF frequency was 1.04 ± 0.01 MHz. Our goal was to induce mild hyperthermia (39−43 °C), a range primarily lethal to cancer cells.[62] Exceeding 45 °C can lead to necrosis in both cancer and surrounding healthy cells and can cause severe vascular stasis, hindering subsequent CT distribution. Thermal camera data obtained during the procedures showed that the HT effect was localized only in the tumor and that over the course of the treatment sessions, maximum tumor surface temperatures of 43.5 ± 2.8 °C were reached, while the body temperatures (as measured by a rectal probe) were kept stable or increased only a few degrees with no direct effect on animal welfare. Overall, tumor HT was well-tolerated at all applied magnetic field strengths, ranging from 4.02 to 7.27 kA/m. As observed in the BxPC-3 bearing mice, none of the treatment groups showed any significant weight loss (Figure S7) or alternative side effects such as loss of appetite, dehydration, lack of voluntary movements upon stimuli or changes in the grooming behavior (see animal monitoring records in Table S4). Temperature increases on the surface of the animal were significant in all three rounds of HT (Figure S8), indicating that the nanoparticles and their heating capability were kept along the experiment.

The efficacy study was designed using suboptimal CT doses in order to better evaluate the additional or synergistic effect of HT. As a result, CT alone had a significant although mild effect on the growth of BxPC-3 tumors compared to untreated mice (p = 0.0328) when tumor volumes were compared 1 week after the last treatment cycle. Remarkably, the combination of CT with the HT had a very significant inhibitory effect on the growth of BxPC-3 s.c. (p = 0.0010) at the same time point (Figure 6b). These results were confirmed upon euthanasia, as tumor weight was lower in mice treated with HT/CT compared with those treated with CT alone (p = 0.0106) (Figure 6c). Concurrently, H−E staining of tumor samples

https://doi.org/10.1021/acsami.4c16129
ACS Appl. Mater. Interfaces XXXX, XXX, XXX−XXX

treated with CT or HT/CT showed a higher number of apoptotic cells and a fainter Ki67 stain (Figure 6d).

Additionally, plasma samples were collected at the end of the treatments to determine the safety of the MNP administration and HT treatment. The results observed a slight trend to increase the hepatic markers such as alanine aminotransferase (ALT) compared to the nontreated group (Table 1). Transient increases in hepatic enzymes in response to MNP-driven HT have been previously observed in experimental animals. In a study by Herrero de la Parte et al.,[63] WAG/RijHsd male rats were subjected to different intensities and frequencies of magnetic field and then euthanized 12 h and 10 days postadministration. While rats exposed to higher doses exhibited increased ALT and AST levels 12 h after HT, these levels returned to baseline by the end of the study, indicating that the damage, if any, was reversible. Transient ALT increases have been also described in response to GEM,[64] and therefore the enhanced GEM accumulation due to the heat might also be behind this increase in ALT levels in the HT/CT group.

Table 1. Serum Biochemical Parameters Assessing Hepatic and Renal Profiles Post-Treatment (Mean ± SEM)[a]

parameter (units)	nontreated	CT	HT/CT
ALT (U/L)	14.07 ± 0.88	15.46 ± 2.53	22.93 ± 4.62
ALP (U/L)	3.55 ± 1.49	3.66 ± 1.05	3.24 ± 2.17
total bilirubin (mg/dL)	0.04 ± 0.03	0.02 ± 0.02	0.07 ± 0.03
glucose (mg/dL)	210.72 ± 18.59	183.03 ± 29.18	196.27 ± 46.04
total protein (g/dL)	3.83 ± 0.31	3.61 ± 0.31	4.22 ± 035
urea (mg/dL)	40.05 ± 0.63	14.07 ± 0.88	45.91 ± 6.69
creatinine (mg/dL)	0.21 ± 0.02	0.15 ± 0.01	0.22 ± 0.03
GGT (U/L)	1.00	1.00	1.00
cholesterol (mg/dL)	76.1 ± 8.03	83.6 ± 13.94	94.50 ± 19.53
P (mg/dL)	3.76 ± 0.86	6.20 ± 0.71	5.03 ± 0.81

[a]ALT, alanine transaminase; ALP, alkaline phosphatase; GGT, γ glutamyltransferase; P, inorganic phosphate.

In agreement with previous *in vitro* results, the combination of HT with CT (GEM/nab-PTX) worked synergistically to reduce tumor burden in BxPC-3 s.c. models. Although combinatorial HT/CT therapies have demonstrated significant suppression of tumor growth in many different preclinical models and also in the clinic,[31,65] there is still no comprehensive understanding of the mechanisms responsible and their interrelationships.[24] At the tumor histology level, there are several players that could explain the observed efficacy of the magnetic HT intervention: direct necrosis, changes in the vasculature, and alteration of the extracellular matrix, among others. Thus, additional histological analyses were conducted to evaluate the effect of the treatment in the stromal compartment and the extension of the necrotic area. The extent of necrotic or neoangiogenic areas in the HT/CT-treated tumors was not greater than in the CT-treated animals, meaning that direct necrosis or changes in the vasculature cannot be responsible for the HT efficacy as the temperature increases are mild. However, Masson's trichrome staining, which labels in blue collagen fibers, showed that tumors dissected from mice treated with HT/CT had significantly less stromal component than those from untreated mice or mice treated with CT alone (Figure 7a). These data were further confirmed with Elastica van Gieson (EVG) staining, visualizing elastic fibers, as an additional component of the extracellular matrix (Figure 7b).

Given that the NTT Agent was mainly located in the stromal component of the tumors, it seems reasonable to hypothesize that the HT directly affected the integrity of this highly dense extracellular matrix, either by disrupting the collagen fibers or by reducing the ability of stromal fibroblasts to produce them. Using iron oxide nanocubes, Kolosnjaj-Tabi et al. demon-

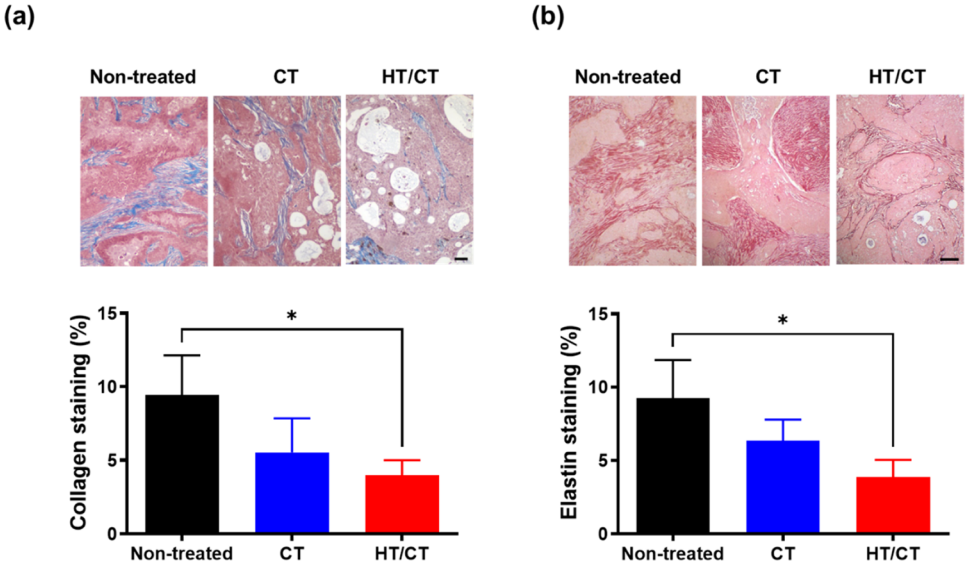

Figure 7. Effect of the combination of HT with CT in the tumor stroma. (a) Masson's trichrome (MT) staining and the quantification of the extension of collagen I (blue color in the MT) staining represented as a percentage to the total area of the tumor. (b) Elastica van Gieson (EVG) staining and the quantification of the extension of elastin (intense pink color). Quantification was performed in $n = 4$ animals/group. The threshold for significance was $P < 0.05$ (*). Magnification bar in the last image corresponds to 50 μm and applies to all images.

https://doi.org/10.1021/acsami.4c16129
ACS Appl. Mater. Interfaces XXXX, XXX, XXX−XXX

strated that nanoparticle-mediated HT induced phase transitions in collagen networks, destabilization of collagen bundles, defibrillation, and subsequent enhanced nanoparticle penetration.[17] In addition, because collagen is the most thrombogenic macromolecular component of the extracellular matrix, disruption of collagen fibers and their release into the circulation could eventually induce a thrombogenic response that would ultimately block further supply of nutrients to the tumor. This hypothesis was supported by proteomic analysis of subcutaneous colorectal tumors treated with combination HT-5FU, where the signaling pathway of GP6, a major collagen receptor, was overrepresented in tumors receiving the combinatorial treatment.[66] Although we did not observe major thrombogenic events in tumors treated with HT/CT, a similar proteomic analysis would be helpful to understand how destabilization of the extracellular matrix affects tumor growth. Finally, a third possible explanation for the higher efficacy for the HT/CT combination could be the immunogenic response of the tumor to the HT. In previous studies, hyperthermia has been reported to modulate local pro-inflammatory responses and immune activation, mostly mediated by heat shock proteins (HSPs), and to also promote immune cell infiltration through increased endothelial cell activation and permeability.[67] Furthermore, in mild HT treatment, endothelial cells showed increased expression of angiopoietin (Angpt) 1 and 2, which stimulated immune cell infiltration.[68] The same phenomena may also occur with the HT/CT combination in pancreatic tumors, as histological analysis of tumor samples revealed a significant presence of histiocytes within the tumors. Whether this increase in histiocytes is also accompanied by an increase in the immunogenic cell death (ICD) requires further investigation.[69,70]

Given the benefits of the combination of different treatment modalities in the management of cancer, future research should be addressed with respect to the development and use of nanomaterials that could combine such effects in a single treatment. This has been already explored with CT-functionalized MNPs[71,72] but alternative combinations such as the photodynamic therapies or the radiotherapy are also very promising for cancer treatment.[73−75]

3. CONCLUSIONS

Overall, efficacy and biodistribution assays demonstrate that the NTT Agent is safe and effective for use as part of the combined HT/CT approach to the treatment of PDAC. On the one hand, our results demonstrate that the HT/CT combination is synergistic, meaning that the HT sensitizes PDAC cells to the treatment with gemcitabine and paclitaxel. On the other hand, *in vivo* experiments have shown the advantages of the HT/CT combination, such as the increase in the efficacy and the reduction of the tumor's desmoplasia.

Importantly, these results supported a successful application for approval by the Spanish Agency of Medicines and Medical Devices (AEMPS) to undertake a clinical safety and feasibility study at the Vall d'Hebron University Hospital in Barcelona, using a multicore variant of the NTT Agent and the combined HT/CT treatment plan described here, in locally advanced PDAC patients. It may well be the case that results of this clinical evaluation, as well as the preclinical data presented in this article, will pave the way for more widespread use of nanoparticle-directed magnetic hyperthermia as adjuvant therapy alongside standard-of-care therapies for future cancer treatments.

4. MATERIALS AND METHODS

4.1. Synthesis and Characterization of the NTT Agent. Maghemite nanoparticles were obtained following a modified Massart coprecipitation protocol.[21,26] Briefly, magnetite (Fe_3O_4) nanoparticles were synthesized by adding, drop by drop at a 0.1 mL/s rate, 75 mL of NH_4OH (25%) solution to 425 mL of an aqueous solution of $FeCl_3{\cdot}6H_2O$ (24.3 g, 0.09 mol) and $FeCl_2{\cdot}4H_2O$ (10.7 g, 0.054 mol). After the addition, the temperature was increased to 90 °C and maintained at that temperature for 3 h. The reaction was allowed to cool to room temperature, and the particles were washed three times with water for injection water and collected with the help of a permanent magnet. Then, the Fe_3O_4 nanoparticles were oxidized to maghemite (γ-Fe_2O_3) by a thermal acid treatment.[76] Briefly, 300 mL of HNO_3 (2 M) was added to a dispersion of the particles in 500 mL of water for injection (WFI) quality water, and the mixture was stirred for 15 min; the supernatant was removed by magnetic decantation. Furthermore, 75 mL of $Fe(NO_3)_3$ (1 M) and 130 mL of WFI water were added to the particles, and the mixture was heated to boiling temperature and stirred for 30 min. The particles were then allowed to cool to room temperature, and by magnetic decantation, the supernatant was substituted by 300 mL of HNO_3 (2 M), and the solution stirred for 15 min. Finally, the particles were washed three times with water for injection.

After nanoparticle synthesis, modification of their surface with dextran was carried out in a thermoregulated ultrasonic bath. Thus, 800 mg of dextran (40 kDa, Panreac Applichem) dissolved in 10 mL of distilled water was added to a dispersion of 800 mg γ-Fe_2O_3 in 2 mL of 2.5 M NaOH. The mixture was sonicated for 10 h at 20 °C and washed by either dialysis or centrifugation using ultracentrifugal filters of 100 kDa. For *in vitro* and *in vivo* testing, coated MNPs were sterilized by gamma radiation (25 kGγ) in Aragogamma (Spain). The pH of the samples was adjusted to 7 and osmolarity was modified with a solution of NaCl 0.9% to 285−310 mOsm/L (OSMOMAT 030, Gonotec).

Nanoparticles were characterized in at least 5 different production batches using different techniques: particle size, shape and size distribution were determined by transmission electron microscopy (TEM); hydrodynamic size, polydispersity index (PdI), and zeta potential of the particles in liquid suspensions were measured by dynamic light scattering (DLS) using a Zetasizer Nano ZS from Malvern Instruments. Heating abilities of magnetic nanoparticles were evaluated through their specific loss powers (SLPs) determining the magnetic losses by AC magnetometry in a portable magnetometer, as previously described.[21] Vibrating sample magnetometry (VSM) was carried out in an MLVSM9Mag Lab 2 T (Oxford Instruments).

4.2. Cell Lines. For *in vitro* studies as well as for generating *in vivo* subcutaneous xenografts, MiaPaCa-2 (CRL-1420) and BxPC-3 (CRL-1687) pancreatic cancer cell lines were obtained from American Type Culture Collection (ATTC, LGC Standards, Barcelona, Spain). MiaPaCa-2 cells were cultured in MEM medium supplemented with 10% fetal bovine serum (FBS, Gibco) and 2.5% horse serum (Gibco), and the BxPC-3 cells were cultured in RPMI medium supplemented with 10% FBS. Cells were kept at 37 °C under a 5% CO_2-saturated atmosphere.

4.3. *In Vitro* Efficacy Assays. For the evaluation of the effect on NTT Agent on MiaPaCa-2 on BxPC-3 cell viability *in vitro*, cells were seeded in culture dishes with 4 wells for self-insertion attached to cell culture dishes of 35 mm. The cells were treated once they reached 60% confluency. Four culture dishes with 4 wells were used for each condition (untreated and NTT) in duplicates to compare the cell viability with and without HT. Cells treated with NTT were incubated with the nanoparticles at 0.5 and 1 mg Fe/mL for 24 h, and then the AMF was applied in the corresponding conditions using the commercial AC field applicator DM100 (nanoscale Biomagnetics) for 20 min with an amplitude of 23.8 kA/m and a frequency of 202 kHz. These experiments were carried out within a thermally insulated

https://doi.org/10.1021/acsami.4c16129
ACS Appl. Mater. Interfaces XXXX, XXX, XXX−XXX

working space at 37 °C. Then, the cells were washed twice with PBS. AlamarBlue assays (Thermo Fisher Scientific) were performed to evaluate the effect of magnetic HT on cell viability the same day that the AMF was applied and the following 2 days. To that end, a stock solution of resazurin sodium salt (1 mg/mL) in PBS was diluted 1% (v/v) in complete Dulbecco's modified Eagle's medium (DMEM) or RPMI medium and added to the cells. After 3 h at 37 °C in the incubator, the fluorescence was measured at 25 °C, λex/em = 550/590 nm (Synergy H4 microplate reader, Biotek), and viability was represented as the percentage, where 100% cell viability corresponded to the untreated cells.[33] For the evaluation of the combination of CT with AMF, the same procedure was followed although using lower doses of nanoparticles. In detail, cells were treated for 24 h with GEM (0.01 μM), PTX (0.01 μM), and NTT at 0.5 mg Fe/mL, and then, AMF was applied as described above.

4.4. *In Vivo* Assays. *4.4.1. Mouse and Tumor Models.* All animal experiments were performed in compliance with the Guide for the Care and Use of Laboratory Animals of the Vall d'Hebron University Hospital and the Fuenlabrada University Hospital and procedures were approved by the corresponding Ethics Committee (CEA-OH/10153 and 77/17, respectively). Mice were housed in individually ventilated cage units and maintained under pathogen-free conditions. Food and water were provided ad libitum.

Six-week old female Hsd:Athymic Nude−Fox mice were subcutaneously injected with 10×10^6 MiaPaCa-2 cells or BxPC-3 cells on the right dorsal back. Studies with these models were performed by the ICTS "NANBIOSIS" of CIBER-BBN's *In vivo* Experimental Platform for Functional Validation & Preclinical Research (FVPR) (www.nanbiosis.es/portofolio/u20-in-vivo-experimental-platform). As for the PDX models, they were generated at the Fuenlabrada University Hospital, following procedures previously described.[49] Subcutaneous (s.c.) tumor size was recorded two times a week by caliper measurements and tumor volume calculated using $(D \times d^2)/2$, where "D" is the largest diameter and "d" the smallest one. When the diameter of the tumors reached 150−300 mm^3 approximately, the mice were randomized in different treatment groups. At the end point, *ex vivo* tumors were weighted and compared among groups. In addition, liver, kidney, spleen, and lung were collected, and half of the tissues were formalin-fixed and embedded in paraffin to perform a histological study by Hematoxylin−eosin (H−E), Masson's trichrome (MT), EVG, or Ki67 staining.

4.4.2. Intratumoral Administration of the NTT Agent. Injection of the NTT Agent was performed in anesthetized mice with a Hamilton syringe (30G). To ensure a constant and continuous flow of MNP in the center of the tumor, the syringe needle was carefully inserted through the skin above the tumor until the needle tip entered the tumor, the push was stopped, and the syringe was clamped to a retort stand. To inject the nanoparticle, the plunger was slowly depressed over 2 min, irrespective of the volume. Once the full volume was injected (1 mg of Fe per 100 mm^3 of tumor), the needle was kept inside the tumor for 2 min, and then slowly withdrawn (1 min).

4.4.3. Magnetic HT Protocol. AMF was applied after MNP administration using a preclinical magnetic HT device, known as the "MACH" system (magnetically alternating current hyperthermia system from Resonant Circuit Limited, London). The device was connected to an ELC Power supply that drove a self-optimizing resonant frequency through a coil and into any MNPs introduced into the field volume. The system was cooled by running water kept at 30 °C by a chiller (Fisher Scientific). To carry out the HT, the mouse was positioned on the cylindrical support of the MACH system, and the tumor was placed in the middle of the coil. Fiber optic probes (Fotemp4, Optocon AG, Dresden, Germany) were used for temperature measurements (rectal and tumor surface). Furthermore, the hot spot temperature of the tumor was recorded with a thermographic camera (Testo 875). HT procedure was carried out increasing the voltage: (i) 15 V during 1 min, (ii) 18 V during 3 min, (iii) 20 V during 3 min, (iv) 24 V during 3 min, and (v) 26 V. In all cases, the AMF frequency was 1.04 MHz. Finally, the procedure was stopped when tumor temperatures reached 48 °C or after 20 min of initiation of the protocol, whichever was encountered first.

4.4.4. CT Treatment. CT treatment in pancreatic tumors included intraperitoneal administration of gemcitabine (GEM) and intravenous administration of nab-paclitaxel (Abraxane, nab-PTX). The chemotherapeutic drugs were administered at suboptimal doses 4 h after HT with the goal of showing the synergic effect combining nanoparticle-mediated HT with the combination of drugs (GEM/PTX). Animals with s.c. MiaPaCa-2 tumors were treated with 10.0 and 5.0 mg/kg of GEM and nab-PTX, respectively (see Figure S4a for dose selection), whereas animals with s.c. BxPC-3 were treated with 50.0 and 10.0 mg/kg of GEM and nab-PTX, respectively, based on the higher resistance of this cell line to GEM and nab-PTX treatment.[77]

4.4.5. GEM Determinations in Tumors by LC-MS/MS. The separation and detection of GEM was performed on a Waters Acquity UltraPerformance Liquid Chromatographic system coupled with a Waters Xevo TQ MS triple quadrupole mass spectrometer (Milford, MA United States).

Separation was achieved on an Acquity UPLC HSS T3 column (2.1 mm × 50 mm, 1.8 μm particle size) from Waters (Milford, United States). A gradient elution program was conducted for chromatographic separation with mobile phase A (Acetonitrile) and mobile phase B (ammonium acetate 10 mM) as follows: 0−0.5 min hold for 5% A, 0.5−5 min from 5 to 40% A, 5−6 min from 60 to 95% A, 6−7.5 min hold for 95% A and 7.5−8.5 min from 95 to 5% A. Pump was operated at a 0.300 mL/min flow rate with an overall run time of 8.5 min. The injection volume was 7.0 μL. The autosampler was held at 6 °C, and the column oven was set up at 40 °C.

The mass spectrometer was operated by using an electrospray source in positive mode. The MRM transition was m/z 264 → 112 for Gemcitabine. The capillary voltage was maintained at 0.5 kV. Argon was used as the collision gas, and flow was 0.17 mL/min. Desolvation temperature was 450 °C with a gas flow of 1100 L/Hr. The system control and data analysis were carried out using MassLynx software (Version 4.1) and processed using the TargetLynxTM program.

GEM working solution was obtained by diluting the GEM standard 1 mg/mL PBS solution in mouse plasma to a final concentration of 100 ng/mL. Seven-point standard calibrators and blank covering the concentration range 0.01−10.0 ng were prepared daily before analysis by diluting GEM working solution in mouse plasma, except for the blank. For each calibration standard, the area of intermediate peak was determined. Linear regression describing the calibration curve was then calculated using a weighting factor of $1/x$ Concentration 2.

4.4.6. Biodistribution Assays. Total iron quantities in organs were determined by ICP-MS and superparamagnetic iron by Electron Paramagnetic Resonance (EPR) following previously described procedures.[78] X-ray CT images were obtained by using a Quantum FX micro-CT instrument (PerkinElmer, Waltham, MA). Incident X-ray tube voltage was set at 50 kVp and amperage was 160 μA. Acquisition time was 4.5 min. Field of view was 30 mm, corresponding to a 0.059 mm spatial resolution. CT scans were performed 24 h postinjection. Reconstruction of the studies was performed with the Quantum FX software (Perking Elmer) and final images were processed with Amide software.[79]

4.4.7. Histological Evaluation. Tumor and tissue samples fixed with formalin were embedded in paraffin and processed for different staining. Hematoxylin−eosin staining was used for the initial histological analysis by trained histopathologists at Biokeralty and TCD. Tumor sections were carefully evaluated for the presence of necrosis, apoptosis, and localization of iron deposits. Moreover, Ki67 staining was also performed using an automated platform (Bond III system, Leica MicroSystems, Newcastle, U.K.). Ki-67 staining was performed using a rabbit monoclonal antibody (MA5-14520, Invitrogen, 1:200 dilution) and the Leica Bond ER2 antigen retrieval for 20 min with the appendix serving as a positive control.

For the analysis of the stromal component, sections from formalin-fixed samples of MiaPaCa-2 and BxPC-3 subcutaneous tumors were stained with MT and EVG. Briefly, for EVG, sections were oxidized with 0.5% acidified potassium permanganate for 5 min followed by bleaching in 1% oxalic acid. After washing in 96% ethanol, sections were incubated in Millers Elastic stain (CN Tech Lab Supplies, UK) for 3 h. Following differentiation, 96% ethanol sections were

https://doi.org/10.1021/acsami.4c16129
ACS Appl. Mater. Interfaces XXXX, XXX, XXX−XXX

counterstained in Van Gieson's Solution (CN Tech Lab Supplies) for 2 min before being blotted dry and covered with Histomount (CN Tech Lab Supplies). MT slides were prepared using Sigma's Trichrome Stain (Masson) Kit, dehydrated, and mounted in DPX mounting media.

In order to quantify collagen or elastin fibers, a global image of each slide sample was taken at 0.5× magnification under Nikon light microscope (Eclipse E800). Each global sample image was then classified into collagen and noncollagen tissue by manual identification using the trainable Weka plugin of ImageJ, yielding binary probability maps with set thresholds. The resulting binary images were then measured to yield % collagen-positive tissue and % collagen-free tissue. Evaluation of MT and EVG staining for collagen and elastin extension was performed in this way for at least 4 mice per group, with the assistance of senior clinical histopathologists.

4.4.8. Statistical Analysis. All of the analyses and graphs were performed using GraphPad Prism 9 software. Statistical analysis consisted in normality data distribution assessment by Kolmogorov–Smirnov test. If data fitted into a normal distribution, unpaired Student's *t* test, for single comparison of means, or one-way analysis of variance (ANOVA) for multiple comparisons was then applied. Otherwise, nonparametric Mann–Whitney test or Tukey test were employed for single and multiple mean comparisons, respectively. The significance threshold was established at $p < 0.05$, and significance levels were schematically assigned: * ($0.01 \leq p < 0.05$), ** ($0.001 \leq p < 0.01$), or *** ($0.0001 \leq p < 0.001$).

■ ASSOCIATED CONTENT

Supporting Information

The Supporting Information is available free of charge at https://pubs.acs.org/doi/10.1021/acsami.4c16129.

Characterization of MNP stability upon short- and long-term storage (Figure S1 and Tables 1–3); effect of the NTT agent and the chemotherapeutic agents (gemcitabine, GEM and paclitaxel, PTX) in the absence of AMF (Figure S2); animal experimentation: setting of the preclinical MACH system; preliminary setup experiments with the MiaPaCa-2 subcutaneous tumors, content of superparamagnetic iron in different tissues of experimental animals, differential heating response of MiaPaCa-2 and BxPC-3 tumors, weight monitoring in efficacy assays and the heating of the BxPC-3 tumors (Figures S2–S8); and animal welfare monitoring in HT/CT procedures (Table S4) (PDF)

■ AUTHOR INFORMATION

Corresponding Authors

Simó Schwartz, Jr. − *Clinical Biochemistry, Drug Delivery & Therapy (CB-DDT), Vall d'Hebron Institute of Research (VHIR), 08035 Barcelona, Spain; Networking Research Center on Bioengineering, Biomaterials and Nanomedicine (CIBER-BBN), 08035 Barcelona, Spain; Servei de Bioquímica, Hospital Universitari Vall d'Hebron, 08035 Barcelona, Spain;* orcid.org/0000-0001-8297-7971; Phone: +34934894055; Email: simo.schwartz@vhir.org

Ibane Abasolo − *Clinical Biochemistry, Drug Delivery & Therapy (CB-DDT), Vall d'Hebron Institute of Research (VHIR), 08035 Barcelona, Spain; Networking Research Center on Bioengineering, Biomaterials and Nanomedicine (CIBER-BBN), 08035 Barcelona, Spain; Functional Validation & Preclinical Research (FVPR), Unit20 ICTS Nanbiosis, Vall d'Hebron Institute of Research (VHIR), 08035 Barcelona, Spain; Servei de Bioquímica, Hospital Universitari Vall d'Hebron, 08035 Barcelona, Spain; Instituto de Química Avanzada de Cataluña (IQAC), CSIC, 08034 Barcelona, Spain;* Present Address: Instituto de Química Avanzada de Cataluña (IQAC), Centro Superior de Investigaciones Científicas (CSIC), C/Jordi Girona 18-26, 08034 Barcelona, Spain; orcid.org/0000-0001-5970-6276; Phone: +34934006165; Email: ibane.abasolo@iqac.csic.es

Authors

Zamira V. Díaz-Riascos − *Clinical Biochemistry, Drug Delivery & Therapy (CB-DDT), Vall d'Hebron Institute of Research (VHIR), 08035 Barcelona, Spain; Networking Research Center on Bioengineering, Biomaterials and Nanomedicine (CIBER-BBN), 08035 Barcelona, Spain; Functional Validation & Preclinical Research (FVPR), Unit20 ICTS Nanbiosis, Vall d'Hebron Institute of Research (VHIR), 08035 Barcelona, Spain*

Monserrat Llaguno-Munive − *Clinical Biochemistry, Drug Delivery & Therapy (CB-DDT), Vall d'Hebron Institute of Research (VHIR), 08035 Barcelona, Spain*

Nuria Lafuente-Gómez − *IMDEA Nanociencia, Unidad Asociada al Centro Nacional de Biotecnología (CSIC), 28049 Madrid, Spain*

Yurena Luengo − *IMDEA Nanociencia, Unidad Asociada al Centro Nacional de Biotecnología (CSIC), 28049 Madrid, Spain*

Sarah Holmes − *Nanomedicine and Molecular Imaging group, Trinity Translational Medicine Institute (TTMI), Trinity College Dublin (TCD), Dublin 8 Dublin, Ireland*

Jeanne Volatron − *Laboratoire Matière et Systèmes Complexes (MSC), UMR 7057 CNRS, Université Paris Diderot, Paris 75205 cedex, France*

Oihane Ibarrola − *BioKeralty Research Institute AIE, 01510 Miñano, Spain*

Sandra Mancilla − *Clinical Biochemistry, Drug Delivery & Therapy (CB-DDT), Vall d'Hebron Institute of Research (VHIR), 08035 Barcelona, Spain; Networking Research Center on Bioengineering, Biomaterials and Nanomedicine (CIBER-BBN), 08035 Barcelona, Spain; Functional Validation & Preclinical Research (FVPR), Unit20 ICTS Nanbiosis, Vall d'Hebron Institute of Research (VHIR), 08035 Barcelona, Spain*

Francesca Sarno − *Grupo de Oncología Traslacional, Hospital Universitario de Fuenlabrada, 28942 Madrid, Spain*

José Javier Aguirre − *BioKeralty Research Institute AIE, 01510 Miñano, Spain*

Sarah Razafindrakoto − *Laboratoire Matière et Systèmes Complexes (MSC), UMR 7057 CNRS, Université Paris Diderot, Paris 75205 cedex, France*

Paul Southern − *Resonant Circuits Limited, London W1S 4BS, U.K.*

Francisco J. Terán − *IMDEA Nanociencia, Unidad Asociada al Centro Nacional de Biotecnología (CSIC), 28049 Madrid, Spain; Unidad Asociada de Nanobiotecnología (CNB-CSIC e IMDEA Nanociencia), 28049 Madrid, Spain; Unidad de Nanomateriales Avanzados, IMDEA Nanociencia (Unidad de I+D+I Asociada al Instituto de Ciencia de Materiales de Madrid, CSIC), 28049 Madrid, Spain;* orcid.org/0000-0002-2466-6208

Anna Keogh − *Department of Histopathology, St. James's Hospital and Trinity College Dublin, Cancer Molecular Diagnostics, Dublin 8 Dublin, Ireland*

Gorka Salas − *IMDEA Nanociencia, Unidad Asociada al Centro Nacional de Biotecnología (CSIC), 28049 Madrid,*

https://doi.org/10.1021/acsami.4c16129
ACS Appl. Mater. Interfaces XXXX, XXX, XXX−XXX

Spain; Unidad Asociada de Nanobiotecnología (CNB-CSIC e IMDEA Nanociencia), 28049 Madrid, Spain; Unidad de Nanomateriales Avanzados, IMDEA Nanociencia (Unidad de I+D+I Asociada al Instituto de Ciencia de Materiales de Madrid, CSIC), 28049 Madrid, Spain; orcid.org/0000-0002-1196-8813

Adriele Prina-Mello − *Nanomedicine and Molecular Imaging group, Trinity Translational Medicine Institute (TTMI), Trinity College Dublin (TCD), Dublin 8 Dublin, Ireland; Laboratory for Biological Characterisation of Advanced Materials (LBCAM), TTMI, School of Medicine, Trinity College Dublin, Dublin 8 Dublin, Ireland; Trinity St. James's Cancer Institute, School of Medicine (TCD) and St. James's Hospital, Dublin 8 Dublin, Ireland;* orcid.org/0000-0002-4371-2214

Juan Carlos Lacal − *Grupo de Oncología Traslacional, Hospital Universitario de Fuenlabrada, 28942 Madrid, Spain; Instituto de Investigaciones Biomédicas (IIB), CSIC, 28029 Madrid, Spain*

Angel del Pozo − *Nanomedicine and Molecular Imaging group, Trinity Translational Medicine Institute (TTMI), Trinity College Dublin (TCD), Dublin 8 Dublin, Ireland*

Quentin A. Pankhurst − *Resonant Circuits Limited, London W1S 4BS, U.K.; Healthcare Biomagnetics Laboratory, University College London, London W1S 4BS, U.K.*

Manuel Hidalgo − *Grupo de Oncología Traslacional, Hospital Universitario de Fuenlabrada, 28942 Madrid, Spain*

Florence Gazeau − *Laboratoire Matière et Systèmes Complexes (MSC), UMR 7057 CNRS, Université Paris Diderot, Paris 75205 cedex, France;* orcid.org/0000-0002-6482-3597

Álvaro Somoza − *IMDEA Nanociencia, Unidad Asociada al Centro Nacional de Biotecnología (CSIC), 28049 Madrid, Spain; Unidad Asociada de Nanobiotecnología (CNB-CSIC e IMDEA Nanociencia), 28049 Madrid, Spain;* orcid.org/0000-0001-9873-435X

Complete contact information is available at: https://pubs.acs.org/10.1021/acsami.4c16129

Author Contributions

Z.V.D.-R: methodology, formal analysis, data curation, investigation, validation, original draft preparation, writing and editing; M.L.-M., N.L.-G., Y.L., S.H., J.V., O.I., S.M., F.S., J.J.A., P.S., F.J.T., A.K., G.S.: methodology, formal analysis, data curation, and writing—review and editing; A.P.-M., J.C.L., A.d.P., Q.A.P., F.G., M.H., A.S., S.S.Jr., I.A.: conceptualization, writing—review and editing, resources, project administration, and funding acquisition. All authors have read and agreed to the published version of the manuscript.

Funding

The described work was carried out within the projects "Nanomedicine Upscaling for Early Clinical Phases of Multimodal Cancer Therapy" (NoCanTher, GA685795) and "Safety testing in the life cycle of nanotechnology-enabled medical technologies for health" (Safe-n-Medtech, GA 814607), both funded by the European Union's Horizon 2020 Research and Innovation program. I.A. thanks the support from the Generalitat de Catalunya (SGR 1173), and A.S. thanks the support from the Spanish Ministerio de Ciencia e Innovación (CEX2020-001039-S and PID2020-119352RB-I00).

Notes

The authors declare no competing financial interest.

■ ACKNOWLEDGMENTS

Part of the *in vivo* work was conducted at the ICTS Nanbiosis, more specifically to the U20 or *in vivo* Experimental Platform of the Functional Validation & Preclinical Research (FVPR) area (http://www.nanbiosis.es/portfolio/u20-in-vivo-experimental-platform/). Maria del Puerto Morales and Sabino Veintemillas Verdaguer (ICMM-CSIC) are gratefully acknowledged for allowing us to use the DM100 AC field applicator for the *in vitro* efficacy experiments. We are also thankful to Prof. Stephen P. Finn, from the Department of Histopathology at St. James's Hospital and Trinity College Dublin, for collaborating in the histopathological evaluation of tumor samples. We also thank the IPGP PARI facility for ICP-MS measurements and Sonia Lajnef and the EPR core facility (UMR8601/CNRS/Université Paris Cité) for EPR experiments. Graphical abstract was created with BioRender.com.

■ ABBREVIATIONS

ALP, alkaline phosphatase; ALT, alanine transaminase; AMF, alternating magnetic field; CT, chemotherapy; DLS, dynamic light scattering; EVG, elastica van Gieson; FFPE, formalin-fixed paraffin embedded; GEM, gemcitabine; GGT, gamma glutamyltransferase; H−E, hematoxylin−eosin; HIPEC, hyperthermic intraperitoneal chemotherapy; HT, hyperthermia; ICD, immunogenic cell death; i.t., intratumoral; i.v., intravenous; MNP, magnetic nanoparticles; MT, Masson's trichrome; nab-PTX, nanoparticle albumin-bound paclitaxel or Abraxane; NTT, NoCanTher thermotherapy; P, inorganic phosphate; PDAC, pancreatic ductal adenocarcinoma; PdI, polydispersity index; PDX, patient-derived xenografts; PTX, paclitaxel; SLP, specific loss power; TEM, transmission electron microscopy; WFI, water for injection

■ REFERENCES

(1) Sung, H.; Ferlay, J.; Siegel, R. L.; Laversanne, M.; Soerjomataram, I.; Jemal, A.; Bray, F. Global Cancer Statistics 2020: GLOBOCAN Estimates of Incidence and Mortality Worldwide for 36 Cancers in 185 Countries. *Ca-Cancer J. Clin.* **2021**, *71* (3), 209−249.

(2) Vincent, A.; Herman, J.; Schulick, R.; Hruban, R. H.; Goggins, M. Pancreatic Cancer. *Lancet* **2011**, *378* (9791), 607−620.

(3) Conroy, T.; Desseigne, F.; Ychou, M.; Bouché, O.; Guimbaud, R.; Bécouarn, Y.; Adenis, A.; Raoul, J.-L.; Gourgou-Bourgade, S.; de la Fouchardière, C.; Bennouna, J.; Bachet, J.-B.; Khemissa-Akouz, F.; Péré-Vergé, D.; Delbaldo, C.; Assenat, E.; Chauffert, B.; Michel, P.; Montoto-Grillot, C.; Ducreux, M.; Groupe Tumeurs Digestives of Unicancer; PRODIGE Intergroup. FOLFIRINOX versus Gemcitabine for Metastatic Pancreatic Cancer. *N. Engl. J. Med.* **2011**, *364* (19), 1817−1825.

(4) Von Hoff, D. D.; Ervin, T.; Arena, F. P.; Chiorean, E. G.; Infante, J.; Moore, M.; Seay, T.; Tjulandin, S. A.; Ma, W. W.; Saleh, M. N.; Harris, M.; Reni, M.; Dowden, S.; Laheru, D.; Bahary, N.; Ramanathan, R. K.; Tabernero, J.; Hidalgo, M.; Goldstein, D.; Van Cutsem, E.; Wei, X.; Iglesias, J.; Renschler, M. F. Increased Survival in Pancreatic Cancer with Nab-Paclitaxel plus Gemcitabine. *N. Engl. J. Med.* **2013**, *369* (18), 1691−1703.

(5) Wang-Gillam, A.; Li, C.-P.; Bodoky, G.; Dean, A.; Shan, Y.-S.; Jameson, G.; Macarulla, T.; Lee, K.-H.; Cunningham, D.; Blanc, J. F.; Hubner, R. A.; Chiu, C.-F.; Schwartsmann, G.; Siveke, J. T.; Braiteh, F.; Moyo, V.; Belanger, B.; Dhindsa, N.; Bayever, E.; Von Hoff, D. D.; Chen, L.-T.; NAPOLI-1 Study Group; et al. Nanoliposomal Irinotecan with Fluorouracil and Folinic Acid in Metastatic Pancreatic

Cancer after Previous Gemcitabine-Based Therapy (NAPOLI-1): A Global, Randomised, Open-Label, Phase 3 Trial. *Lancet* **2016**, *387* (10018), 545−557.
(6) Miyamoto, R.; Oda, T.; Hashimoto, S.; Kurokawa, T.; Inagaki, Y.; Shimomura, O.; Ohara, Y.; Yamada, K.; Akashi, Y.; Enomoto, T.; Kishimoto, M.; Yanagihara, H.; Kita, E.; Ohkohchi, N. Cetuximab Delivery and Antitumor Effects Are Enhanced by Mild Hyperthermia in a Xenograft Mouse Model of Pancreatic Cancer. *Cancer Sci.* **2016**, *107* (4), 514−520.
(7) Annese, T.; Tamma, R.; Ruggieri, S.; Ribatti, D. Angiogenesis in Pancreatic Cancer: Pre-Clinical and Clinical Studies. *Cancers* **2019**, *11* (3), 381.
(8) Awasthi, N.; Zhang, C.; Schwarz, A. M.; Hinz, S.; Wang, C.; Williams, N. S.; Schwarz, M. A.; Schwarz, R. E. Comparative Benefits of Nab-Paclitaxel over Gemcitabine or Polysorbate-Based Docetaxel in Experimental Pancreatic Cancer. *Carcinogenesis* **2013**, *34* (10), 2361−2369.
(9) De Dosso, S.; Siebenhüner, A. R.; Winder, T.; Meisel, A.; Fritsch, R.; Astaras, C.; Szturz, P.; Borner, M. Treatment Landscape of Metastatic Pancreatic Cancer. *Cancer Treat Rev.* **2021**, *96*, No. 102180.
(10) Paulson, A. S.; Tran Cao, H. S.; Tempero, M. A.; Lowy, A. M. Therapeutic Advances in Pancreatic Cancer. *Gastroenterology* **2013**, *144* (6), 1316−1326.
(11) Thiesen, B.; Jordan, A. Clinical Applications of Magnetic Nanoparticles for Hyperthermia. *Int. J. Hyperthermia* **2008**, *24*, 467.
(12) Sardari, D.; Verg, N.Cancer Treatment with Hyperthermia. In *Current Cancer Treatment - Novel Beyond Conventional Approaches*; InTech, 2011 DOI: 10.5772/24049.
(13) Kolosnjaj-Tabi, J.; Marangon, I.; Nicolas-Boluda, A.; Silva, A. K. A.; Gazeau, F. Nanoparticle-Based Hyperthermia, a Local Treatment Modulating the Tumor Extracellular Matrix. *Pharmacol. Res.* **2017**, *126*, 123.
(14) Kossatz, S.; Grandke, J.; Couleaud, P.; Latorre, A.; Aires, A.; Crosbie-Staunton, K.; Ludwig, R.; Dähring, H.; Ettelt, V.; Lazaro-Carrillo, A.; Calero, M.; Sader, M.; Courty, J.; Volkov, Y.; Prina-Mello, A.; Villanueva, A.; Somoza, Á.; Cortajarena, A. L.; Miranda, R.; Hilger, I. Efficient Treatment of Breast Cancer Xenografts with Multi-functionalized Iron Oxide Nanoparticles Combining Magnetic Hyperthermia and Anti-Cancer Drug Delivery. *Breast Cancer Res.* **2015**, *17*, No. 66, DOI: 10.1186/s13058-015-0576-1.
(15) Sanhaji, M.; Göring, J.; Couleaud, P.; Aires, A.; Cortajarena, A. L.; Courty, J.; Prina-Mello, A.; Stapf, M.; Ludwig, R.; Volkov, Y.; Latorre, A.; Somoza, Á.; Miranda, R.; Hilger, I. The Phenotype of Target Pancreatic Cancer Cells Influences Cell Death by Magnetic Hyperthermia with Nanoparticles Carrying Gemicitabine and the Pseudo-Peptide NucAnt. *Nanomed. Nanotechnol. Biol. Med.* **2019**, *20*, No. 101983.
(16) Piehler, S.; Wucherpfennig, L.; Tansi, F. L.; Berndt, A.; Quaas, R.; Teichgraeber, U.; Hilger, I. Hyperthermia Affects Collagen Fiber Architecture and Induces Apoptosis in Pancreatic and Fibroblast Tumor Hetero-Spheroids in Vitro. *Nanomedicine* **2020**, *28*, No. 102183.
(17) Kolosnjaj-Tabi, J.; Di Corato, R.; Lartigue, L.; Marangon, I.; Guardia, P.; Silva, A. K. A.; Luciani, N.; Clément, O.; Flaud, P.; Singh, J. V.; Decuzzi, P.; Pellegrino, T.; Wilhelm, C.; Gazeau, F. Heat-Generating Iron Oxide Nanocubes: Subtle "Destructurators" of the Tumoral Microenvironment. *ACS Nano* **2014**, *8* (5), 4268−4283.
(18) Hannon, G.; Tansi, F. L.; Hilger, I.; Prina-Mello, A. The Effects of Localized Heat on the Hallmarks of Cancer. *Adv. Ther.* **2021**, *4* (7), No. 2000267.
(19) Nicolas-Boluda, A.; Laurent, G.; Bazzi, R.; Roux, S.; Donnadieu, E.; Gazeau, F. Two Step Promotion of a Hot Tumor Immune Environment by Gold Decorated Iron Oxide Nanoflowers and Light-Triggered Mild Hyperthermia. *Nanoscale* **2021**, *13* (44), 18483−18497.
(20) Nicolás-Boluda, A.; Vaquero, J.; Laurent, G.; Renault, G.; Bazzi, R.; Donnadieu, E.; Roux, S.; Fouassier, L.; Gazeau, F. Photothermal Depletion of Cancer-Associated Fibroblasts Normalizes Tumor Stiffness in Desmoplastic Cholangiocarcinoma. *ACS Nano* **2020**, *14* (5), 5738−5753.
(21) Luengo, Y.; Díaz-Riascos, Z. V.; García-Soriano, D.; Teran, F. J.; Artés-Ibáñez, E. J.; Ibarrola, O.; Somoza, Á.; Miranda, R.; Schwartz, S.; Abasolo, I.; Salas, G. Fine Control of In Vivo Magnetic Hyperthermia Using Iron Oxide Nanoparticles with Different Coatings and Degree of Aggregation. *Pharmaceutics* **2022**, *14* (8), 1526.
(22) Kok, H. P.; Cressman, E. N. K.; Ceelen, W.; Brace, C. L.; Ivkov, R.; Grüll, H.; Ter Haar, G.; Wust, P.; Crezee, J. Heating Technology for Malignant Tumors: A Review. *Int. J. Hyperthermia* **2020**, *37* (1), 711−741.
(23) Egea-Benavente, D.; Ovejero, J. G.; Morales, M. D. P.; Barber, D. F. Understanding MNPs Behaviour in Response to AMF in Biological Milieus and the Effects at the Cellular Level: Implications for a Rational Design That Drives Magnetic Hyperthermia Therapy toward Clinical Implementation. *Cancers* **2021**, *13* (18), 4583.
(24) Etemadi, H.; Plieger, P. G. Magnetic Fluid Hyperthermia Based on Magnetic Nanoparticles: Physical Characteristics, Historical Perspective, Clinical Trials, Technological Challenges, and Recent Advances. *Adv. Ther.* **2020**, *3* (11), No. 2000061.
(25) Spanish Agency of Medicines and Medical Devices (AEMPS). Clinical Trial (797/20/EC): "Clinical Feasibility Study of the Intratumoral Injection of Magnetic Nanoparticles Associated with the Treatment of Hyperthermia in Locally Advanced Pancreatic Cancer for Magnetic Hyperthermia of Locally Advanced Pancreatic Adenocarcinomas", 2020.
(26) Massart, R. Preparation of Aqueous Magnetic Liquids in Alkaline and Acidic Media. *IEEE Trans. Magn.* **1981**, *17*, 1247.
(27) Tansi, F. L.; Maduabuchi, W. O.; Hirsch, M.; Southern, P.; Hattersley, S.; Quaas, R.; Teichgräber, U.; Pankhurst, Q. A.; Hilger, I. Deep-Tissue Localization of Magnetic Field Hyperthermia Using Pulse Sequencing. *Int. J. Hyperthermia* **2021**, *38* (1), 743−754.
(28) Maduabuchi, W. O.; Tansi, F. L.; Faenger, B.; Southern, P.; Pankhurst, Q. A.; Steiniger, F.; Westermann, M.; Hilger, I. Local Magnetic Hyperthermia and Systemic Gemcitabine/Paclitaxel Chemotherapy Triggers Neo-Angiogenesis in Orthotopic Pancreatic Tumors without Involvement of Auto/Paracrine Tumor Cell VEGF Signaling and Hypoxia. *Cancers* **2024**, *16* (1), 33.
(29) Roussel, T.; Ferry, D.; Kosta, A.; Miele, D.; Sandri, G.; Tansi, F. L.; Steiniger, F.; Southern, P.; Pankhurst, Q. A.; Peng, L.; Giorgio, S. Insight into the Internal Structure of High-Performance Multicore Magnetic Nanoparticles Used in Cancer Thermotherapy. *ACS Mater. Au* **2024**, *4* (5), 489−499.
(30) Colombo, M.; Carregal-Romero, S.; Casula, M. F.; Gutiérrez, L.; Morales, M. P.; Böhm, I. B.; Heverhagen, J. T.; Prosperi, D.; Parak, W. J. Biological Applications of Magnetic Nanoparticles. *Chem. Soc. Rev.* **2012**, *41* (11), 4306−4334.
(31) Wust, P.; Hildebrandt, B.; Sreenivasa, G.; Rau, B.; Gellermann, J.; Riess, H.; Felix, R.; Schlag, P. M. Hyperthermia in Combined Treatment of Cancer. *Lancet Oncol.* **2002**, *3* (8), 487−497.
(32) Rao, W.; Deng, Z.-S.; Liu, J. A Review of Hyperthermia Combined with Radiotherapy/Chemotherapy on Malignant Tumors. *Crit Rev. Biomed. Eng.* **2010**, *38* (1), 101−116.
(33) Lafuente-Gómez, N.; Milán-Rois, P.; García-Soriano, D.; Luengo, Y.; Cordani, M.; Alarcón-Iniesta, H.; Salas, G.; Somoza, Á. Smart Modification on Magnetic Nanoparticles Dramatically Enhances Their Therapeutic Properties. *Cancers* **2021**, *13* (16), 4095.
(34) Torres-Lugo, M.; Rinaldi, C. Thermal Potentiation of Chemotherapy by Magnetic Nanoparticles. *Nanomedicine* **2013**, *8* (10), 1689−1707.
(35) Lepock, J. R. Cellular Effects of Hyperthermia: Relevance to the Minimum Dose for Thermal Damage. *Int. J. Hyperthermia* **2003**, *19* (3), 252−266.
(36) Hilger, I.; Rapp, A.; Greulich, K.-O.; Kaiser, W. A. Assessment of DNA Damage in Target Tumor Cells after Thermoablation in Mice. *Radiology* **2005**, *237* (2), 500−506.

https://doi.org/10.1021/acsami.4c16129
ACS Appl. Mater. Interfaces XXXX, XXX, XXX−XXX

(37) Cheng, D.; Li, X.; Zhang, G.; Shi, H. Morphological Effect of Oscillating Magnetic Nanoparticles in Killing Tumor Cells. *Nanoscale Res. Lett.* **2014**, *9* (1), No. 195.
(38) Domenech, M.; Marrero-Berrios, I.; Torres-Lugo, M.; Rinaldi, C. Lysosomal Membrane Permeabilization by Targeted Magnetic Nanoparticles in Alternating Magnetic Fields. *ACS Nano* **2013**, *7* (6), 5091−5101.
(39) Master, A. M.; Williams, P. N.; Pothayee, N.; Pothayee, N.; Zhang, R.; Vishwasrao, H. M.; Golovin, Y. I.; Riffle, J. S.; Sokolsky, M.; Kabanov, A. V. Remote Actuation of Magnetic Nanoparticles For Cancer Cell Selective Treatment Through Cytoskeletal Disruption. *Sci. Rep.* **2016**, *6*, No. 33560.
(40) Huang, H.; Delikanli, S.; Zeng, H.; Ferkey, D. M.; Pralle, A. Remote Control of Ion Channels and Neurons through Magnetic-Field Heating of Nanoparticles. *Nat. Nanotechnol.* **2010**, *5* (8), 602−606.
(41) Mannix, R. J.; Kumar, S.; Cassiola, F.; Montoya-Zavala, M.; Feinstein, E.; Prentiss, M.; Ingber, D. E. Nanomagnetic Actuation of Receptor-Mediated Signal Transduction. *Nat. Nanotechnol.* **2008**, *3* (1), 36−40.
(42) Sandre, O.; Genevois, C.; Garaio, E.; Adumeau, L.; Mornet, S.; Couillaud, F. In Vivo Imaging of Local Gene Expression Induced by Magnetic Hyperthermia. *Genes* **2017**, *8* (2), 61.
(43) Moros, M.; Idiago-López, J.; Asín, L.; Moreno-Antolín, E.; Beola, L.; Grazú, V.; Fratila, R. M.; Gutiérrez, L.; de la Fuente, J. M. Triggering Antitumoural Drug Release and Gene Expression by Magnetic Hyperthermia. *Adv. Drug Delivery Rev.* **2019**, *138*, 326−343.
(44) de Sousa Cavalcante, L.; Monteiro, G. Gemcitabine: Metabolism and Molecular Mechanisms of Action, Sensitivity and Chemoresistance in Pancreatic Cancer. *Eur. J. Pharmacol.* **2014**, *741*, 8−16.
(45) Lim, P. T.; Goh, B. H.; Lee, W.-L. 3 - Taxol: Mechanisms of Action against Cancer, an Update with Current Research. In *Paclitaxel*; Swamy, M. K.; Pullaiah, T.; Chen, Z.-S., Eds.; Academic Press, 2022; pp 47−71 DOI: 10.1016/B978-0-323-90951-8.00007-2.
(46) Tansi, F. L.; Fröbel, F.; Maduabuchi, W. O.; Steiniger, F.; Westermann, M.; Quaas, R.; Teichgräber, U. K.; Hilger, I. Effect of Matrix-Modulating Enzymes on The Cellular Uptake of Magnetic Nanoparticles and on Magnetic Hyperthermia Treatment of Pancreatic Cancer Models In Vivo. *Nanomaterials* **2021**, *11* (2), 438.
(47) Beola, L.; Asín, L.; Fratila, R. M.; Herrero, V.; de la Fuente, J. M.; Grazú, V.; Gutiérrez, L. Dual Role of Magnetic Nanoparticles as Intracellular Hotspots and Extracellular Matrix Disruptors Triggered by Magnetic Hyperthermia in 3D Cell Culture Models. *ACS Appl. Mater. Interfaces* **2018**, *10* (51), 44301−44313.
(48) Ademaj, A.; Veltsista, D. P.; Ghadjar, P.; Marder, D.; Oberacker, E.; Ott, O. J.; Wust, P.; Puric, E.; Hälg, R. A.; Rogers, S.; Bodis, S.; Fietkau, R.; Crezee, H.; Riesterer, O. Clinical Evidence for Thermometric Parameters to Guide Hyperthermia Treatment. *Cancers* **2022**, *14* (3), 625.
(49) Izumchenko, E.; Paz, K.; Ciznadija, D.; Sloma, I.; Katz, A.; Vasquez-Dunddel, D.; Ben-Zvi, I.; Stebbing, J.; McGuire, W.; Harris, W.; Maki, R.; Gaya, A.; Bedi, A.; Zacharoulis, S.; Ravi, R.; Wexler, L. H.; Hoque, M. O.; Rodriguez-Galindo, C.; Pass, H.; Peled, N.; Davies, A.; Morris, R.; Hidalgo, M.; Sidransky, D. Patient-Derived Xenografts Effectively Capture Responses to Oncology Therapy in a Heterogeneous Cohort of Patients with Solid Tumors. *Ann. Oncol.* **2017**, *28* (10), 2595−2605.
(50) Martinez-Garcia, R.; Juan, D.; Rausell, A.; Muñoz, M.; Baños, N.; Menéndez, C.; Lopez-Casas, P. P.; Rico, D.; Valencia, A.; Hidalgo, M. Transcriptional Dissection of Pancreatic Tumors Engrafted in Mice. *Genome Med.* **2014**, *6* (4), No. 27.
(51) Rubio-Viqueira, B.; Jimeno, A.; Cusatis, G.; Zhang, X.; Iacobuzio-Donahue, C.; Karikari, C.; Shi, C.; Danenberg, K.; Danenberg, P. V.; Kuramochi, H.; Tanaka, K.; Singh, S.; Salimi-Moosavi, H.; Bouraoud, N.; Amador, M. L.; Altiok, S.; Kulesza, P.; Yeo, C.; Messersmith, W.; Eshleman, J.; Hruban, R. H.; Maitra, A.; Hidalgo, M. An in Vivo Platform for Translational Drug Development in Pancreatic Cancer. *Clin. Cancer Res.* **2006**, *12* (15), 4652−4661.
(52) Pestieau, S. R.; Stuart, O. A.; Chang, D.; Jacquet, P.; Sugarbaker, P. H. Pharmacokinetics of Intraperitoneal Gemcitabine in a Rat Model. *Tumori J.* **1998**, *84* (6), 706−711.
(53) García-Santos, E. P.; Padilla-Valverde, D.; Villarejo-Campos, P.; Murillo-Lázaro, C.; Fernández-Grande, E.; Palomino-Muñoz, T.; Rodríguez-Martínez, M.; Amo-Salas, M.; Nuñez-Guerrero, P.; Sánchez-García, S.; Puerto-Puerto, A.; Martín-Fernández, J. The Utility of Hyperthermic Intra-Abdominal Chemotherapy with Gemcitabine for the Inhibition of Tumor Progression in an Experimental Model of Pancreatic Peritoneal Carcinomatosis, in Relation to Their Behavior with Pancreatic Cancer Stem Cells CD133+ CXCR4. *Pancreatology* **2016**, *16* (4), 632−639.
(54) Kossatz, S.; Ludwig, R.; Dähring, H.; Ettelt, V.; Rimkus, G.; Marciello, M.; Salas, G.; Patel, V.; Teran, F. J.; Hilger, I. High Therapeutic Efficiency of Magnetic Hyperthermia in Xenograft Models Achieved with Moderate Temperature Dosages in the Tumor Area. *Pharm. Res.* **2014**, *31*, 3274.
(55) Levy, M.; Luciani, N.; Alloyeau, D.; Elgrabli, D.; Deveaux, V.; Pechoux, C.; Chat, S.; Wang, G.; Vats, N.; Gendron, F.; Factor, C.; Lotersztajn, S.; Luciani, A.; Wilhelm, C.; Gazeau, F. Long Term in Vivo Biotransformation of Iron Oxide Nanoparticles. *Biomaterials* **2011**, *32* (16), 3988−3999.
(56) Hannon, G.; Bogdanska, A.; Keogh, A.; Finn, S. P.; Gobbo, O. L.; Prina-Mello, A. Biodistribution and Histological Analysis of Iron Oxide-Dextran Nanoparticles in Wistar Rats. *Nanotoxicology* **2023**, *17* (8−9), 562−580.
(57) Beola, L.; Grazú, V.; Fernández-Afonso, Y.; Fratila, R. M.; Heras, M. d. l.; Fuente, J. M. d. l.; Gutiérrez, L.; Asín, L. Critical Parameters to Improve Pancreatic Cancer Treatment Using Magnetic Hyperthermia: Field Conditions, Immune Response, and Particle Biodistribution. *ACS Appl. Mater. Interfaces* **2021**, *13* (11), 12982−12996.
(58) Kim, D.-H.; Guo, Y.; Zhang, Z.; Procissi, D.; Nicolai, J.; Omary, R. A.; Larson, A. C. Temperature-Sensitive Magnetic Drug Carriers for Concurrent Gemcitabine Chemohyperthermia. *Adv. Healthcare Mater.* **2014**, *3* (5), 714−724.
(59) Taurin, S.; Nehoff, H.; Greish, K. Anticancer Nanomedicine and Tumor Vascular Permeability; Where Is the Missing Link? *J. Controlled Release* **2012**, *164* (3), 265−275.
(60) Man, F.; Lammers, T.; Rosales, R. T. M. de. Imaging Nanomedicine-Based Drug Delivery: A Review of Clinical Studies. *Mol. Imaging Biol.* **2018**, *20*, 683−695, DOI: 10.1007/s11307-018-1255-2.
(61) Dadfar, S. M.; Roemhild, K.; Drude, N. I.; von Stillfried, S.; Knüchel, R.; Kiessling, F.; Lammers, T. Iron Oxide Nanoparticles: Diagnostic, Therapeutic and Theranostic Applications. *Adv. Drug Delivery Rev.* **2019**, *138*, 302−325.
(62) Hegyi, G.; Szigeti, G. P.; Szász, A. Hyperthermia versus Oncothermia: Cellular Effects in Complementary Cancer Therapy. *Evidence-Based Complementary Altern. Med.* **2013**, *2013*, No. 672873.
(63) Herrero de la Parte, B.; Rodrigo, I.; Gutiérrez-Basoa, J.; Iturrizaga Correcher, S.; Mar Medina, C.; Echevarría-Uraga, J. J.; Garcia, J. A.; Plazaola, F.; García-Alonso, I. Proposal of New Safety Limits for In Vivo Experiments of Magnetic Hyperthermia Antitumor Therapy. *Cancers* **2022**, *14* (13), 3084.
(64) Gemcitabine. *LiverTox: Clinical and Research Information on Drug-Induced Liver Injury*; National Institute of Diabetes and Digestive and Kidney Diseases: Bethesda (MD), 2012.
(65) Issels, R. D. Hyperthermia Adds to Chemotherapy. *Eur. J. Cancer* **2008**, *44* (17), 2546−2554.
(66) Dabaghi, M.; Rasa, S. M. M.; Cirri, E.; Ori, A.; Neri, F.; Quaas, R.; Hilger, I. Iron Oxide Nanoparticles Carrying 5-Fluorouracil in Combination with Magnetic Hyperthermia Induce Thrombogenic Collagen Fibers, Cellular Stress, and Immune Responses in Heterotopic Human Colon Cancer in Mice. *Pharmaceutics* **2021**, *13* (10), 1625.
(67) Lee, S.; Son, B.; Park, G.; Kim, H.; Kang, H.; Jeon, J.; Youn, H.; Youn, B. Immunogenic Effect of Hyperthermia on Enhancing Radiotherapeutic Efficacy. *Int. J. Mol. Sci.* **2018**, *19* (9), 2795.

https://doi.org/10.1021/acsami.4c16129
ACS Appl. Mater. Interfaces XXXX, XXX, XXX−XXX

(68) Li, M.; Fuchs, S.; Böse, T.; Schmidt, H.; Hofmann, A.; Tonak, M.; Unger, R.; Kirkpatrick, C. J. Mild Heat Stress Enhances Angiogenesis in a Co-Culture System Consisting of Primary Human Osteoblasts and Outgrowth Endothelial Cells. *Tissue Eng., Part C* **2014**, *20* (4), 328−339.
(69) Zhang, L.; Zhang, Q.; Hinojosa, D. T.; Jiang, K.; Pham, Q.-K.; Xiao, Z.; Colvin, V. L.; Bao, G. Multifunctional Magnetic Nanoclusters Can Induce Immunogenic Cell Death and Suppress Tumor Recurrence and Metastasis. *ACS Nano* **2022**, *16* (11), 18538−18554.
(70) Yan, B.; Liu, C.; Wang, S.; Li, H.; Jiao, J.; Lee, W. S. V.; Zhang, S.; Hou, Y.; Hou, Y.; Ma, X.; Fan, H.; Lv, Y.; Liu, X. Magnetic Hyperthermia Induces Effective and Genuine Immunogenic Tumor Cell Death with Respect to Exogenous Heating. *J. Mater. Chem. B* **2022**, *10* (28), 5364−5374.
(71) Dabaghi, M.; Quaas, R.; Hilger, I. The Treatment of Heterotopic Human Colon Xenograft Tumors in Mice with 5-Fluorouracil Attached to Magnetic Nanoparticles in Combination with Magnetic Hyperthermia Is More Efficient than Either Therapy Alone. *Cancers* **2020**, *12* (9), 2562.
(72) Rezaei, B.; Yari, P.; Sanders, S. M.; Wang, H.; Chugh, V. K.; Liang, S.; Mostufa, S.; Xu, K.; Wang, J.-P.; Gómez-Pastora, J.; Wu, K. Magnetic Nanoparticles: A Review on Synthesis, Characterization, Functionalization, and Biomedical Applications. *Small* **2024**, *20* (5), No. e2304848.
(73) Mignani, S.; Bryszewska, M.; Klajnert-Maculewicz, B.; Zablocka, M.; Majoral, J.-P. Advances in Combination Therapies Based on Nanoparticles for Efficacious Cancer Treatment: An Analytical Report. *Biomacromolecules* **2015**, *16* (1), 1−27.
(74) Zhang, C.; Xia, D.; Liu, J.; Huo, D.; Jiang, X.; Hu, Y. Bypassing the Immunosuppression of Myeloid-Derived Suppressor Cells by Reversing Tumor Hypoxia Using a Platelet-Inspired Platform. *Adv. Funct. Mater.* **2020**, *30* (22), No. 2000189.
(75) Dinakaran, D.; Wilson, B. C. The Use of Nanomaterials in Advancing Photodynamic Therapy (PDT) for Deep-Seated Tumors and Synergy with Radiotherapy. *Front. Bioeng. Biotechnol.* **2023**, *11*, No. 1250804.
(76) Costo, R.; Bello, V.; Robic, C.; Port, M.; Marco, J. F.; Puerto Morales, M.; Veintemillas-Verdaguer, S. Ultrasmall Iron Oxide Nanoparticles for Biomedical Applications: Improving the Colloidal and Magnetic Properties. *Langmuir* **2012**, *28*, 178.
(77) Fryer, R. A.; Barlett, B.; Galustian, C.; Dalgleish, A. G. Mechanisms Underlying Gemcitabine Resistance in Pancreatic Cancer and Sensitisation by the iMiD Lenalidomide. *Anticancer Res.* **2011**, *31* (11), 3747−3756.
(78) Kolosnjaj-Tabi, J.; Javed, Y.; Lartigue, L.; Volatron, J.; Elgrabli, D.; Marangon, I.; Pugliese, G.; Caron, B.; Figuerola, A.; Luciani, N.; Pellegrino, T.; Alloyeau, D.; Gazeau, F. The One Year Fate of Iron Oxide Coated Gold Nanoparticles in Mice. *ACS Nano* **2015**, *9* (8), 7925−7939.
(79) Loening, A. M.; Gambhir, S. S. AMIDE: A Free Software Tool for Multimodality Medical Image Analysis. *Mol. Imaging* **2003**, *2*, 131.

https://doi.org/10.1021/acsami.4c16129
ACS Appl. Mater. Interfaces XXXX, XXX, XXX−XXX